Spring 1-1-2015

An Investigation into Establishing a Formation of Small Satellites in a Lunar Flower Constellation

Lauren McManus
University of Colorado at Boulder, lamc9987@colorado.edu

An Investigation into Establishing a Formation of Small Satellites in a Lunar Flower Constellation

by

Lauren McManus

B.E., Auburn University, 2013

A thesis submitted to the

Faculty of the Graduate School of the

University of Colorado in partial fulfillment

of the requirements for the degree of

Masters of Science

Department of Aerospace Engineering

2015

This thesis entitled:
An Investigation into Establishing a Formation of Small Satellites in a Lunar Flower Constellation
written by Lauren McManus
has been approved for the Department of Aerospace Engineering

Hanspeter Schaub

Prof. Jeff Parker

Prof. Dan Scheeres

Date

The final copy of this thesis has been examined by the signatories, and we find that both the content and the form meet acceptable presentation standards of scholarly work in the above mentioned discipline.

McManus, Lauren (MS, Astrodynamics and Satellite Navigation)

An Investigation into Establishing a Formation of Small Satellites in a Lunar Flower Constellation

Thesis directed by Prof. Hanspeter Schaub

Lunar science missions such as LADEE and GRAIL achieved unprecedented measurements of the Lunar exosphere and gravity field. These missions were performed with one (LADEE) or two (GRAIL) traditional satellites. The global coverage achieved by these missions could have been greatly enhanced with the use of a constellation of satellites. A constellation of communication satellites at the Moon would also be necessary if a Lunar human base were to be established. Constellations with many satellites are expensive with traditional technology, but have become feasible through the technological advancements and affordability of cubesats. Cubesat constellations allow for full surface coverage in science or communication missions at a reasonable mission cost.

Repeat ground track orbits offer interesting options for science or communication constellations, since they provide repeat coverage of the surface at a fixed time between sequential visits. Flower constellations are a family of constellations being studied primarily by Daniele Mortari at Texas A&M University that make use of repeat ground tracks. Orbital parameters are selected such that the nodal period of the orbit matches the nodal period of the primary body by a factor dependent on the number of days and the number of revolutions to repeat the ground track. All orbits in a flower constellation have identical orbital elements, with the exception of the right ascension of the ascending node (RAAN) and the initial mean anomaly, which are determined based on the desired phasing scheme desired.

Flower constellations have thus far primarily been studied at Earth. A flower constellation at the Moon could be quite useful for science or communication purposes. In this scenario, the flower constellation satellites would be small satellites, which introduces many unique challenges. The cubesats would have limited propulsion capability and would need to be deployed from a mothercraft. Orbital maintenance would then be required after deployment to retain the repeat

ground track nature of flower constellations. The limited fuel on the cubesats and the maneuvers required determine the lifetime of the constellation. The communications range of the cubesats will also be limited; following a successful deployment, the mothercraft must move into a long-term communications orbit where it can see both the children craft and Earth, to act as a communications relay.

This work investigates the differences in flower constellations at the Moon versus at Earth. It is found that due to the longer rotation period of the Moon, the number of petals in the flower constellation must be quite large in order to produce reasonable orbit sizes. Two types of flower constellations are investigated: a single-petal and multi-petal constellation. The single-petal constellation consists of a string-of-pearls formation within one inertial flower constellation orbit. The multi-petal configuration has one satellite per inertial orbit, with the orbits spaced symmetrically within a 360° RAAN distribution. Optimal methods for deployment are explored for both configurations. Phasing orbits are used to deploy the single-petal constellation. This is found to be a simple and low-cost deployment scheme. The multi-petal configuration requires larger plane change maneuvers, and three-burn transfer orbit solutions that are optimal over single impulsive burn maneuvers are found. The mothercraft maneuver into the long-term communications orbit is also investigated. This maneuver is once again just a phase orbit maneuver for the single-petal constellation and is low cost. A polar mothercraft orbit is desired for the multi-petal configuration, again requiring a large and expensive plane change maneuver. As was the case with the deployment maneuver, a three-burn transfer orbit series is found to be cost optimal over a series of impulsive burns for this maneuver. Finally, once the constellation is established, orbit maintenance maneuvers are calculated. A 4 kg cubesat with 1 kg of fuel is assumed, and various thruster types are used to correlate required maintenance ΔVs to propellant mass required. It is found that the flower constellations at the Moon can be maintained for between 100 and 800 days, depending on the efficiency of the thruster system used. Ultimately, a small satellite constellation at the Moon is found to be feasible to establish and maintain for a science or communication mission.

Dedication

I would like to dedicate this thesis to my family who has always been supportive of me in everything that I do. I would especially like to thank my mom who has tirelessly edited every paper that I have ever produced, including this thesis. While she claims to no longer understand the majority of the material that I write about, her attention to detail is unparalleled and has been much appreciated in both my undergraduate and graduate studies. My sister is my best friend and was my constant cheerleader throughout this process and my father made sure I still had fun and "embraced college". I would also like to thank the amazing friend group that I have acquired in just a couple of short years in Boulder. This experience would not have been the same without them!

Acknowledgements

I would like to acknowledge my advisor, Dr. Hanspeter Schaub, for his support of this thesis. Through countless meetings, we developed many of the ideas of this work and his guidance has been critical to my success. I would also like to thank Dr. Jeff Parker for his willingness to share his expertise on the Moon and Dr. Dan Scheeres in his assistance in optimization techniques. I would also like to acknowledge the support of Ann Smead and Michael Byram for their generous financial support in the form of the Joseph H. Smead Fellowship, as well as the intangible support and mentorship that they provide for the Smead Fellows. This work was primarily funded by the National Science Foundation Graduate Research Fellowship Program, award number DGE 1144083.

Contents

Chapter

Tables

Table

Figures

Figure

Chapter 1

Introduction

1.1 Motivation

The Scientific Context for Exploration of the Moon (SCEM) report produced by the National Research Council includes studies of the lunar atmosphere and dust environment as one of eight major priorities for future lunar science missions [6]. In fact, the Moon is considered to be a key to deciphering the evolutionary history of planets because it preserves a surface record spanning most of solar system history and it very accessible from Earth [19]. In addition to lunar science missions, there are also plans to return humans to the Moon and establish a lunar base, which would require a communication satellite structure. A satellite constellation at the Moon is proposed as a configuration for potential science or communications missions. Small satellites, such as cubesats, are great candidates for such a constellation due to the affordable nature of cubesats. Despite the aforementioned benefits, there are still many challenges associated with establishing a constellation of small satellites at the Moon.

A constellation at the Moon faces many unique challenges that are not present for a constellation at Earth. For an Earth-based constellation, satellites can be launched individually over time, as was done with the GPS constellation. Therefore, the satellites could be launched near to their desired orbit planes, avoiding the need for large, expensive plane change maneuvers. Conversely, for a constellation of small satellites about the Moon, the satellites would be deployed from a mothercraft once at the Moon as launching all constellation satellites to the Moon individually would be too costly. A lunar flower constellation concept is shown in Fig. 1.1. Three of the four

cubesats have already been deployed into their orbits and the mothercraft has just deployed the final satellite. The orbits shown are in the inertial frame.

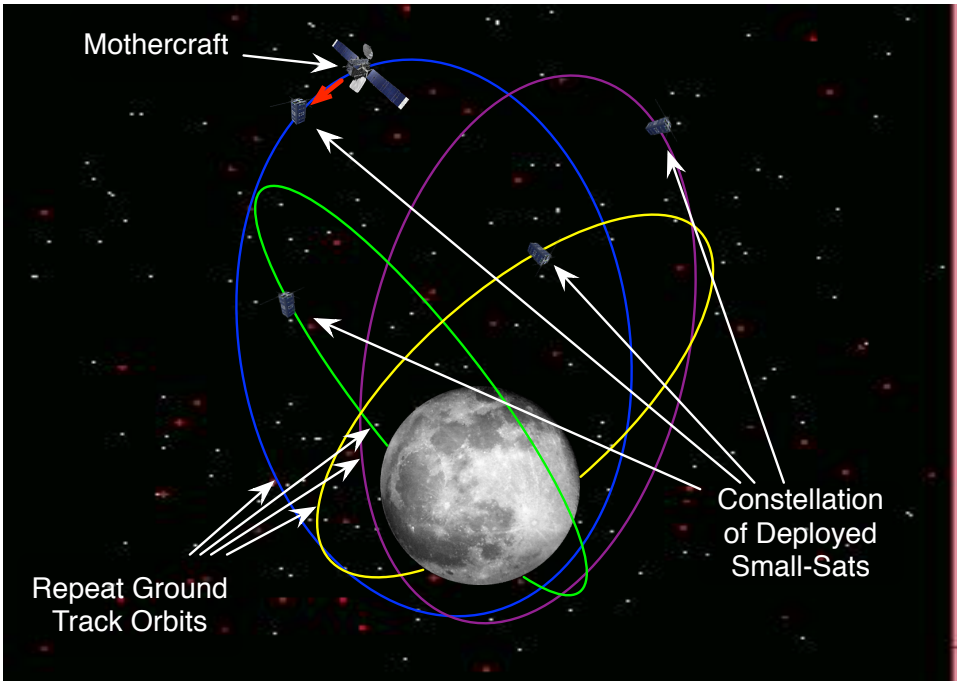

Figure 1.1: Small satellites in a lunar flower constellation deployed by mothercraft

Once the constellation is established, satellites at the Moon will experience quite different perturbations than those experienced by satellites at Earth. Certain perturbations from the non-sphericity of the Moon and Earth will be present for both Moon- and Earth-based constellations. However, which perturbations dominate varies between the Earth and the Moon. At Earth, the perturbations tend to be more predictable, whereas perturbations at the Moon are strongly influenced by the irregular gravity field of the Moon and third-body effects, with these perturbations highly dependent on the orbit geometry.

1.2 Literature Review

1.2.1 Lunar Missions

Exploration to the Moon began before the Apollo era. Early observations allowed for a basic understanding of the lunar surface and composition. Further missions have been necessary, however, in order to better characterize the structure of the Moon. There were several missions to the Moon in the 1970s and 1990s and they continue today since the evolutionary reconstruction of the Moon is a key science goal, as it is believed that the Moon preserves a surface record that spans most of the solar system history [19]. The Moon is also very accessible from Earth, making lunar missions easy and affordable as compared to exploring other planets. Three of these missions are briefly presented in this section.

The lunar Atmosphere and Dust Environment Explorer (LADEE) was a low-cost lunar orbiter that measured the atmosphere and dust environment at the Moon in 2013 to 2014. This mission was in alignment with The National Research Council report, *The Scientific Context for Exploration of the Moon* (SCEM), which listed studying the lunar atmosphere and dust environment as one of eight major priorities for future lunar science missions [6]. The lunar atmosphere is actually an exosphere (collision-less gas of neutral atoms), and much of it is unexplored [6]. LADEE had two major science goals in exploring the dynamic lunar exosphere. The first goal was to investigate the composition of the exosphere, as well as the source and sink processes that create the distribution and variability in the exosphere; the second goal was to characterize the dust environment [6]. LADEE is just one satellite in NASA's portfolio of near-term lunar missions to explore the Moon before humans return to the surface and potentially disturb the lunar environment [6].

Another successful lunar science mission was the Gravity Recovery and Interior Laboratory (GRAIL). This mission mapped the gravity field of the Moon in 2011 to 2012. The GRAIL mission had two identical satellites flying in a leader-follower formation, similar to the Earth based gravity field mapping mission known as GRACE. Mapping was accomplished with the lunar Gravity Ranging System (LGRS), which measured the distance between the two GRAIL satellites [19].

The distance between the two satellites varied as the spacecraft were perturbed by the irregular lunar surface; the change in separation distance measured by the LGRS was used to reconstruct the gravity field. The gravity field produced from GRAIL's mapping is up to spherical harmonic degree and order 420[19]. In addition to providing an improved gravity field, the GRAIL mission also discerned new structures on the Moon. These features include tectonic structures, volcanic landforms, basin rings, crater central peaks, and many craters[19].

The Japanese Kaguya (SELENE) mission to the Moon from 2007 to 2009 was a pioneer mission to explore the Moon, enabling future lunar studies and utilization[15]. The mission tasks included determining the elemental and mineral composition of the Moon, observing the lunar topography, measuring the gravity field of the far side of the Moon, and studying the effect of solar radiation on the Moon[15]. This mission is particularly interesting because like GRAIL, it utilized multiple satellites. However, it differs from GRAIL in that there were a total of three satellites, and the main orbiter carried the two subsatellites on its roof to the Moon where they were then released into their own orbits[15]. The two subsatellites were a relay satellite named Okina and a very-long-baseline interferometry (VLBI) satellite called Ouna. Okina and Ouna were released as Kaguya lowered its apoapsis into to its nominal orbit value. The Kaguya spacecraft intentionally impacted the Moon in June 2009 and Okina impacted later that year once fuel resources were exhausted. Interestingly, Ouna has still not impacted the Moon and while the orbit varies vastly, the periapsis altitude has yet to dip to below the surface of the Moon and will not crash anytime in the near future, although telemetry command was terminated after Kaguya impacted.

LADEE, GRAIL, and Kaguya are just three examples of lunar missions to contribute to the key science goal of the evolutionary reconstruction of the Moon. LADEE and GRAIL involved traditionally sized spacecraft, with one craft for LADEE and two for GRAIL. Kaguya was unique in that it involved one traditional main craft and two small (57 kg) subsatellites. While all three missions were successful, the lunar coverage of a science mission could be vastly improved by further increasing the number of satellites in the mission. A larger formation or a constellation could be used to achieve global coverage and affordable cubesats could be the solution to providing this

coverage at a reasonable mission cost.

1.2.2 Small Satellite Constellations

Constellations are a new application for cubesats. The first, and only, cubesat constellation is the Flock constellation from Planetary Labs. These cubesats are launched to the ISS and then inserted into orbit using the Nanotracks deployment system [1]. This was the first constellation deployment from the ISS. This constellation will eventually consist of 200 satellites and is being launched in phases, with 43 satellites already deployed [1]. The Flock satellites will provide Earth imagery with complete coverage of the Earth. A constellation of this size is only made possible by advances in small satellite capabilities, as it would have been prohibitively expensive with traditional satellite systems. There still exist some trade-offs between spacecraft size and functionality, but advances in miniaturization and integration technologies have eliminated many of the sacrifices that previously accompanied reduced size spacecraft [1]. The lower development costs and shorter lead times, combined with the increased capabilities of cubesats, make them very desirable candidates for constellations. The Flock mission has demonstrated the advantages of cubesats, causing other missions to look to cubesats for global coverage capabilities.

The QB50 mission aims to establish a constellation of 50 cubesats that will take measurements of Earth's lower thermosphere. This proposed mission is slightly more advanced than the Flock constellation because it involves two special satellites within the 50 that have additional propulsion capability in order to maintain a formation flying scheme. Formation flying has not yet been achieved with cubesats. Some small satellite formation flying has been explored: The Prisma mission flew a 145 kg and 45 kg satellite in formation, and the SNAP-1 6.5 kg and Tsinghua-1 50 kg spacecraft attempted formation flying [5]. The QB50 formation flying mission will require attitude control and propulsion systems with advanced performance capability for a cubesat, considering that many cubesats do not have any attitude or propulsion capabilities at all. For a cubesat constellation to be maintained for any amount of time, a good attitude and propulsion system is necessary. The work of QB50 will help to validate the technology readiness levels (TRLs) of these

components, enabling more applications for cubesats than ever before.

While the trade-offs between cubesat size and capability have been greatly reduced, the limited capabilities of cubesats do still present many challenges. There are still very restricted budgets for cubesat mass, volume, and power, as well as technologies and capabilities when compared to traditional satellites[5]. The limited propellant directly reduces the satellite lifetime and the type of feasible maneuvers. In particular, significant orbit plane changes are likely not feasible with cubesats[5]. This is the most significant challenge in the deployment of a constellation of cubesats. The best solution is to deploy the satellites into orbits near their desired orbits, so that any large maneuvers can be avoided. The decreased technological capabilities do somewhat limit the scientific research that can be achieved by a single small satellite. However, this problem can be addressed with the combination of many satellites with identical sensors into larger constellations or formations, where many fundamental science questions can be addressed[5]. Ultimately, not only are cubesats the only cost effective way to create very large constellations, cubesats actually perform best when combined into a constellation or formation. The pairing of small satellites and multi-satellite architectures is, therefore, both advantageous and a natural partnership.

1.2.3 Lunar Frozen Orbits

Due to the limited fuel available in cubesats, constellation orbits that utilize the natural perturbations of the primary body to reduce station-keeping maneuvers over time are highly desirable. These orbits are often referred to as frozen. In general, a frozen orbit is an orbit with specific orbital parameters that allow any one or more orbital parameters to be fixed, even under the effects of perturbations. The perturbations vary based on the central body. Since the current work is investigating a constellation of small satellites at the Moon, a brief review of frozen orbit work at the Moon is presented.

Frozen orbits about the Moon typically refer to orbits at a specified combination of semi-major axis, eccentricity, and/or inclination such that the mean eccentricity and argument of periapsis remain constant over time[4]. Lunar frozen orbits are very dependent on the distribution of lunar

mascons and third-body effects from the Earth[4]. As was previously mentioned, the primary disturbances for Earth orbits are due to the J_2 through J_5 terms. Considering only second-order zonal harmonics (J_2), frozen orbits can be found analytically using the expressions from Vallado for secular drift rates, as given by Eq. (1.1)[16]. The term J_2 accounts for the oblateness of the primary body. For Earth, J_2 is 0.00108236 and for the Moon it has a value of 0.00020433.

$$\dot{\Omega} = -\frac{3nR_{\text{eq}}^2 J_2}{2p^2}\cos i \tag{1.1a}$$

$$\dot{\omega} = \frac{3nR_{\text{eq}}^2 J_2}{4p^2}\left(4 - 5\sin^2 i\right) \tag{1.1b}$$

$$\dot{M}_0 = -\frac{3nR_{\text{eq}}^2 J_2\sqrt{1-e^2}}{4p^2}\cos i\left(2\sin^2 i - 2\right) \tag{1.1c}$$

In Eq. (1.1), $p = a(1-e^2)$ is the orbital parameter–also known as the semilatus rectum–and R_{eq} is the equatorial radius of the primary body. Frozen inclinations are found by setting Eq. (1.1b) to zero. It can be seen that once Eq. (1.1b) is set to zero, it reduces to the form:

$$4 - 5\sin^2 i = 0 \tag{1.2}$$

From Eq. (1.2), it can be seen that there is no dependence on any other orbital parameters or planetary constants. Therefore, the frozen inclinations of 63.4° and 116.6° that satisfy Eq. (1.2) hold for any orbit around any primary body when only second order zonal harmonics are considered in designing a frozen orbit. However, for the Moon, J_2 is not strongly dominant and the effects from the mascons and Earth cannot be ignored. In fact, it is found that frozen orbits at the Moon are dependent upon other orbit elements in addition to the inclination. Frozen orbit solutions are also dependent upon the method by which they are found.

In Reference 4, Folta and Quinn search for lunar frozen orbits through examining combinations of inclination, semi-major axis, and eccentricity to either completely eliminate or control the drift in the mean eccentricity and argument of periapsis. Lagrange's planetary equations along with a forcing function that describes the averaged effect of third-body disturbances at the Moon are used to find frozen orbits where one or more orbit element drifts are zeroed out. It was found

that equatorial orbits ($i = 0°, 180°$) eliminate RAAN drift ($\dot{\Omega}$). This is considered a trivial solution since RAAN is undefined for equatorial orbits. Instead, solutions where $\dot{e}$ goes to zero with ω equal to either 0°, 90°, 180°, or 270° are used[4]. In addition to an elimination of the eccentricity drift, the drift in the argument of periapsis should ideally be removed, as well. In order to drive $\dot{\omega}$ to zero for $\omega = 0°, 180°$, the eccentricity becomes 1.0 and a parabolic escape orbit is created[4]. An escape orbit is not desirable for a frozen orbit, so only arguments of periapsis of 90° and 270° are used for further investigation. As will be discussed later, these happen to also be the desired arguments of periapsis for flower constellations. A simple expression for the eccentricity as a function of the frozen inclination is derived[4]:

$$e = \left(1 - \frac{5}{3}\cos i^2\right)^{\frac{1}{2}} \tag{1.3}$$

Equation (1.3) can be used in flower constellation design at the Moon. Rather than using the J_2 frozen inclinations of 63.4° and 116.6°–which satisfy Eq. (1.2)–a third-body frozen inclination can be found using Eq. (1.3) with the eccentricity desired for the flower constellation. It is important to note, however, that this frozen inclination is an estimate for third-body effects and does not account for the irregular gravity field of the Moon. Despite this deficiency, it is a more realistic calculation than that derived using only second-order zonal harmonics and will likely reduce station-keeping efforts in the lifetime of the constellation.

In Reference 3, a differing approach to finding lunar frozen orbits that accounts for the non-sphericity of the Moon is used. However, this is still an approximate method as only the oblateness of the Moon (J_2) and equatorial ellipticity (C_{22}) are used to account for the first and second order of the disturbing potential. An analytical expression for a critical inclination which sets $\dot{\omega}$ to zero is found[3]:

$$\cos i^2 = \frac{\varepsilon + \delta \cos h}{5(\varepsilon + 2\delta \cos h)} \tag{1.4a}$$

$$\varepsilon = J_2 R_{\mathrm{m}}^2 \tag{1.4b}$$

$$\delta = -C_{22} R_{\mathrm{m}}^2 \tag{1.4c}$$

Where Delaunay canonical variables are used rather than the typical Keplerian orbital elements.

Therefore, h is simply the RAAN, Ω. This method for finding critical inclinations only eliminates the drift in the argument of periapsis since the J_2 and C_{22} coefficients do not affect the eccentricity rate in Lagrange's planetary equations[3]. A frozen inclination that eliminates both $\dot{\omega}$ and $\dot{e}$ is far more desirable. A further disadvantage of this method is that Eq. (3.3a) creates a dependence of the frozen inclination on the h, or the RAAN. This makes this method infeasible for a flower constellation since all flower constellation orbits must be at the same inclination despite being at different RAANs.

The ardent research activity surrounding stable frozen orbits about the Moon and other bodies is driven by the advantages that frozen orbits can offer once realized. Frozen orbits could allow for for decreased fuel costs as station-keeping maneuvers are minimized or ideally, eliminated. Additionally, frozen orbits provide useful configurations for science or communications missions as the orbits are repeatable and lend themselves well to potential repeat ground track configurations.

1.2.4 Repeat Ground Track Orbits

Repeat ground track (RGT) orbits are very desirable for many of the science missions mentioned in Sections 1.2.1 and 1.2.2. RGT configuration would enable the same surfaced to be revisited repeatedly, with a fixed elapsed time between visits. Repeat ground tracks are created when the nodal period of the orbit matches the nodal period of the primary body. Vallado defines the nodal period as the elapsed time between two consecutive equator crossings[16]. The nodal period of the Moon is the period of the Moon's rotation as measured from the ascending node of a satellite's orbit[16]:

$$T_{\Omega_M} = \frac{2\pi}{\omega_B - \dot{\Omega}} \tag{1.5}$$

Where ω_B is the rotation rate of the primary body (2.6619×10^{-6} rad/s for the Moon and 7.2722×10^{-5} rad/s for the Earth) and $\dot{\Omega}$ is the drift rate in RAAN. When the nodal period of the orbit and the nodal period of the primary body do not match, the ground tracks produced will have offsets between consecutive equator crossings. This offset, called the ground track shift, is based on how much the body rotates relative to the drift in the orbit's ascending node[16]. When a ground track

is designed to repeat after one orbit, the nodal period of the orbit exactly matches the nodal period of the primary body, such that there is no ground track shift. In order for a repeat ground track orbit to hold up over time without controls, it must also be a frozen orbit, so that the argument of periapsis remains constant.

Russell and Lara in Reference 12 investigated long-lifetime repeat ground track orbits at the Moon, expanding on investigations of repeat ground tracks at Europa. Periodic solutions where the normalized period of the orbit exactly matched one period of the Moon's revolution plus the additional change in the longitude of the ascending node of the orbit were desired[12]. This is in effect matching the nodal period of the orbit to the period of the Moon's rotation, as described in Eq. (1.5).

In order to capture a realistic lunar orbit environment, Russell and Lara used the lp150q model of the lunar gravity field along with the Earth-Moon restricted three-body problem (RTBP). However, the Earth-Moon RTBP is still only an approximation and does not hold up for an arbitrary lunar gravity field[12]. Stable and near-stable solutions for periodic orbits are successfully found for various input parameters. However, due to the approximations made by the RTBP, the exact repeating ground tracks found do not hold up over time. This destruction of the repeat ground tracks are found to be a function of the orbit altitude. As the altitude increases, the approximations from the RTBP become more detrimental[12]. Similar to most reasonable approximations, control laws and station-keeping thrusting can be used to compensate for these mis-modeled dynamics.

Interestingly, the results of Reference 12 were merely families of solutions for frozen orbits. The solutions could be near-circular or eccentric and were not confined to any specific inclination. The characteristic that most distinguished these families of frozen repeat ground track orbits was the integer ratio of orbit revolutions to revolutions of the Moon during the period of repetition for the ground track[12]. The number of orbit revolutions varied from 73 to 328 cycles, while the revolution of the Moon was held to one. The value of 328 cycles provides for a low altitude two hour period orbit, and the value of 73 cycles was chosen somewhat arbitrarily to provide an orbit altitude around two lunar radii[12].

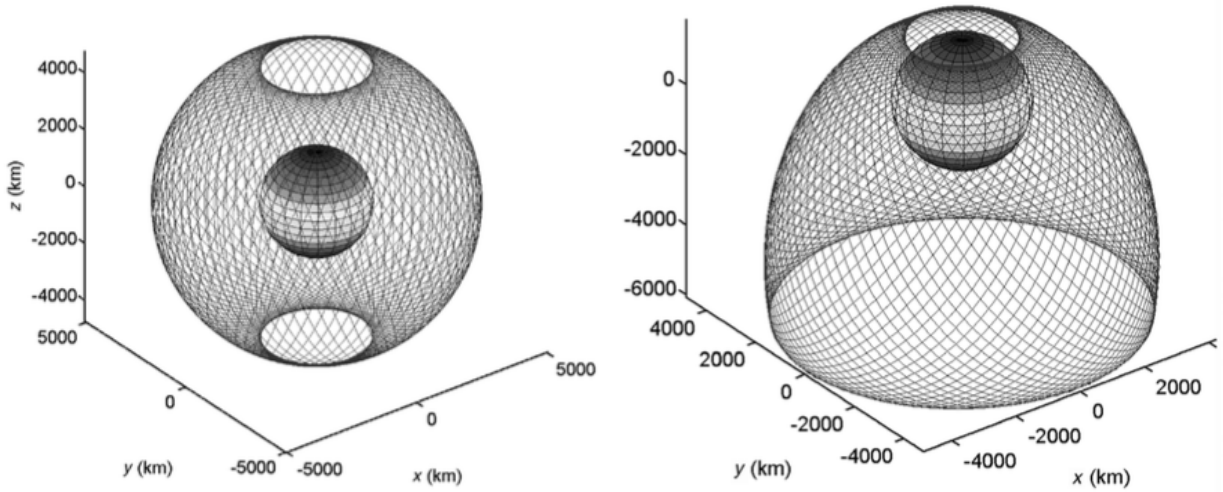

(a) Near-circular 73-cycle

(b) Eccentric 73-cycle

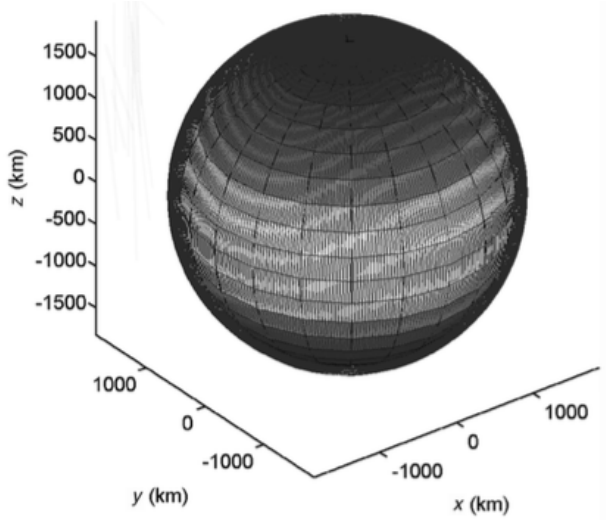

(c) Near-circular 328-cycle

Figure 1.2: RGT relative orbits[12]

It can be seen in Fig. 1.2 the effect that the eccentricity and number of cycles to repeat can have on the relative orbits for a repeat ground track orbit. As the number of cycles to repeat increases, the semi-major axis decreases and the orbits go from high-altitude orbits to low-altitude orbits, as can be seen through comparing Fig. 1.2c and Fig. 1.2a. The near circular orbits are also symmetric about both the spin-axis of the Moon and the equator as shown in Fig. 1.2a, whereas the equatorial symmetry is lost with the eccentric orbit shown in Fig. 1.2b. It is important to note

that these RGT orbits are for a specific unique combination of orbital elements.

These repeat ground track orbits are fundamentally based in frozen orbits but match the nodal periods of the orbit to the rotation period of the Moon. This is the core concept behind a type of RGT constellation called flower constellations.

1.2.5 Flower Constellations

Flower constellations are a unique family of constellations being studied primarily by Daniele Mortari at Texas A&M University. Flower constellations are characterized by their repeat ground tracks and their axis of symmetry. Orbital parameters are selected based on matching the nodal period of the orbit with the nodal period of the central body about which the constellation is orbiting. Scale factors for the number of days and the number of revolutions to repeat the ground tracks determine the period of repetition for the constellation [11]:

$$T_{\mathrm{r}} = N_{\mathrm{p}} T_{\Omega} = N_{\mathrm{d}} T_{\Omega_{\mathrm{B}}} \tag{1.6}$$

In Eq. (1.6), T_{r} is the period of repetition for the ground tracks, N_{p} is the number of revolutions to repeat, T_{Ω} is the nodal period of the orbit, N_{d} is the number of days to repeat, and T_{Ω_B} is the nodal period of the primary body. Another important parameter in flower constellations is the number of satellites, N_{s}. Flower constellations are named based on three parameters as N_{p}-N_{d}-N_{s} constellations.

The relationship given for the nodal period in Eq. (1.6) can lead to an expression for the anomalistic period, from which the orbit eccentricity and semi-major axis can be found. The number of satellites in the orbit (N_{s}), the number of days to repeat (N_{d}), and the number of revolutions to repeat (N_{p}) are all inputs for a given flower constellation. All orbits in the constellation are identical, but rotated at different right ascensions of the ascending node (RAANs). The inclination, argument of periapsis, and the height of periapsis for the orbits are also designer inputs, along with the initial mean anomaly and RAAN of the first satellite in the constellation.

All previous work with flower constellations has studied the constellations at Earth. Flower

constellations at the Moon could be very useful for science and communications purposes. The primary difference between an Earth and Moon based flower constellation is that the satellites in an Earth based constellation would likely be launched individually over time, similar to how the GPS constellation was constructed. Due to the high cost of going to the Moon, however, a lunar flower constellation would ideally consist of small satellites that are deployed from one mothercraft once at the Moon. These small satellites would have limited to no propulsion ability so the mothercraft would do the majority of the maneuvering in the deployment. Flower constellations are typically characterized by an axis of symmetry aligned with the spin axis of the central body. The orbits are typically created to be radially symmetric about this axis of symmetry by evenly distributing the RAANs. The current study will look at optimal methods to achieve the desired RAAN distribution for a flower constellation since large plane change maneuvers may be required.

Flower constellations have many applications, including communication, space observation, global positioning systems, and formation flying[11]. The key component of flower constellations is their repeat ground tracks. They are also designed to be J_2 compatible. The development of flower constellations is based upon matching the nodal period of the orbit to the nodal period of the primary body and will be presented in detail in the following chapter.

1.3 Scope of Research

The current study investigates deploying and maintaining a flower constellation of small satellites at the Moon. There are many challenges associated with applying flower constellations to the Moon instead of the Earth. The dominant perturbation at Earth is J_2, and flower constellations are inherently designed to be J_2 compatible. Therefore, perturbations are not a significant concern when studying flower constellations at the Earth. However, the perturbations at the Moon are far less predictable. Lunar orbits are highly impacted by third-body effects from Earth as well as the irregular gravity field of the lunar surface. These perturbations affect various orbits uniquely, and can affect an individual satellite differently throughout its orbital period. These additional perturbations present unique challenges that must be overcome in order to maintain a flower constellation

at the Moon.

In addition to the differing perturbations at Earth and the Moon, the rotation periods are drastically different between the two bodies. The Earth completes one rotation every 24 sidereal hours, whereas the Moon takes 27.32 Earth days to revolve. The large period of the Moon's rotation creates flower constellations with very large periods of repetition, and therefore, orbit periods, as given by the relationship in Es. (1.6). The parameters N_{p} and/or N_{d} must, therefore, be adjusted to compensate for the large nodal period of the Moon, resulting in a reasonable orbit period and thus semi-major axis. These alterations will dramatically affect the appearance of flower constellations at the Moon, but do not change the fundamental principles behind these elegant repeat ground track configurations. This will be further explored in Chapter 2.

Besides the challenges presented by the lunar rotation period and perturbations, the establishment of any constellation at the Moon takes an entirely different form than it would at Earth. As stated above, a constellation can be built at Earth through a process of individual satellite launches over time. At the Moon, this is not a cost-effective means by which to create a constellation. Instead, a mothercraft would be employed to release small satellites (such as cubesats) into the constellation configuration. These satellites would have limited propulsion capability, and, therefore, the mothercraft must be responsible for the majority, if not all, of the maneuvering in such a deployment scheme. The constellation satellites can then conserve their fuel to be used for station-keeping maneuvers throughout the constellation lifetime.

Two primary deployment schemes are investigated in the current study. The first scheme is for a single petal flower constellation. The advantage of this constellation is that all satellites lie in a single plane. Therefore, this formation lends itself to a simple deployment scheme where the mothercraft releases all the children craft from a raised orbit. These two configurations are shown in Fig. 1.3.

The second deployment scheme investigates the mothercraft maneuvers necessary to achieve the proper RAAN distribution for a multi-petal flower constellation with orbit planes symmetrically spaced within a full 360° RAAN range. This is a more complicated deployment process than the

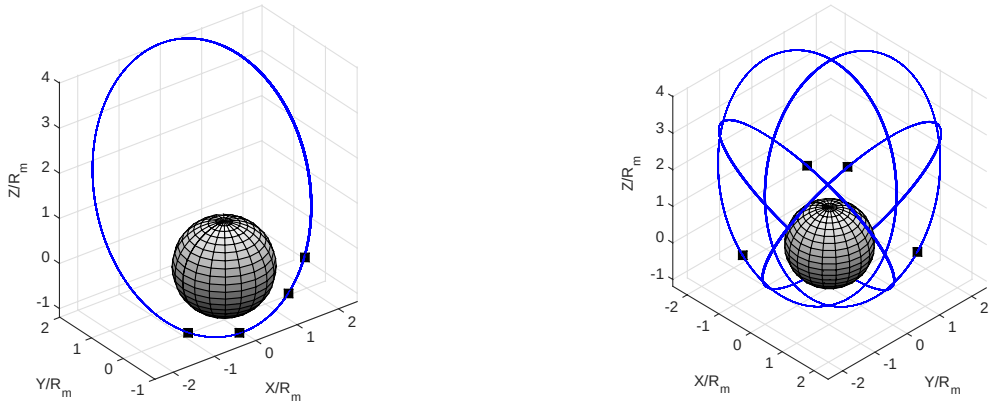

(a) Single-petal FC

(b) Multi-petal FC

Figure 1.3: Flower constellation configuration inertial orbits

SOP formation. A series of single impulsive burns to change the inclination and RAAN are used as a baseline cost. An optimized three-burn transfer trajectory that minimizes fuel cots is desired to complete the maneuvers between sequential planes within the flower constellation. Ultimately, these two deployment schemes can be used together to create formations within a full symmetric flower constellation.

The mothercraft serves a variety of functions throughout the lifetime of a flower constellation at the Moon. Initially, the mothercraft is the transport vehicle by which the constellation satellites travel to the Moon from the Earth. Once at the Moon, the mothercraft is fully responsible for the deployment of the flower constellation satellites. Once the constellation is established, the mothercraft takes on the role of a communications relay between the flower constellation satellites and the Earth.

The long-term communications orbit of the mothercraft will be a function of the flower constellation configuration used. The requirements for the mothercraft orbit are that it either be in view of all children craft at all times or travels by all children craft periodically. The first option is more feasible in a single petal formation configuration where all children satellites are within close proximity to one another. The second option would be necessary for a multi-petal constellation

as the mothercraft would no longer be able to see all children craft simultaneously. Instead, the mothercraft would need to be on an orbit with a different period (i.e., different semi-major axis) than the flower constellation orbits so that it will travel by all satellites in the constellation.

An alternative long-term orbit for the mothercraft could also be a halo orbit at the L1 or L2 libration points. A large halo orbit at L1 or L2 would allow the mothercraft to see all flower constellation satellites while they pass along either the Earth-side or the back-side of the Moon, respectively. Any L1 halo orbit would always be able to see and communicate with the Earth, and a large enough L2 orbit that avoids obstruction by the Moon could also be seen by the Earth at all times.

A flower constellation at the Moon would be subject to strong perturbative effects from the Earth and the irregular lunar gravity field. To maintain the exact repeat ground tracks characteristic of a flower constellation, a frozen orbit is needed. While frozen orbits have been shown to exist at the Moon, they are dependent upon a unique combination of orbit elements and are, therefore, not compatible with a flower constellation where all orbits must share the same elements with the exception of the RAAN. Therefore, when implemented at the Moon, flower constellation orbit elements will drift over time and require an impulsive control strategy to mitigate these precessions. Some drift is actually desired, as flower constellations are designed to be J_2 compatible. In other words, the controls will be used to eliminate all precession that results from perturbations other than J_2. Therefore, second order frozen inclinations of 63.4° and 116.6°, which satisfy Eq. (1.2), will serve as the desired inclinations for flower constellations at the Moon. At these inclinations, the argument of periapsis drift due to J_2 goes to zero. The drift in RAAN is compensated for by the orbital period and repeat ground tract nature of flower constellations. While the additional perturbations at the Moon will cause the orbit to precess from this desired orbit, the control laws will compensate for those effects. The control ΔV required to maintain the flower constellation configuration will be investigated in order to predict the constellation lifetime.

Chapter 2

Applying Flower Constellations to the Moon

2.1 Flower Constellation Setup

As previously mentioned, flower constellations can be very useful for science missions that require observation of the lunar surface due to the nature of their repeat groundtracks. The orbital elements for the satellites in a flower constellation are dependent upon matching the period of repetition for the constellation to the period of rotation of the central body, as well as to the desired spacing of the satellites. The flower constellation development presented in this chapter will be specific to a flower constellation at the Moon, rather than at a different central body, such as Earth.

2.1.1 Period Matching

Flower constellations are fundamentally based on the concept of repeatable ground tracks. The ground tracks are designed for repetition after a specified number of revolutions (N_p) and a specified number of days (N_d), as given by Eq. (1.6). The number of days to repeat is defined as a day for the primary body. In other words, one day is one rotation of the primary body. The Moon takes 27.32 Earth days to complete one rotation, so that an N_d of one lunar day corresponds to 27.32 Earth days. From Eq. (1.6), a relationship for the anomalistic period needs to be found. The anomalistic period is the periapsis-to-periapsis period that is defined by the familiar period equation[16]:

$$T = 2\pi\sqrt{\frac{a^3}{\mu}} \tag{2.1}$$

Where a is the semi-major axis and μ is the gravitational parameter for the Moon ($4902.799\ km^3/s^2$). The relationship between the nodal period and the anomalistic period is [11]:

$$T = T_\Omega \left(1 + \frac{\dot{M}_0 + \dot{\omega}}{n}\right) \tag{2.2}$$

In Eq. (2.2), $n = \sqrt{\mu/a^3}$ is the mean motion and $\dot{M}_0$ and $\dot{\omega}$ are the drift rates in the initial mean anomaly and the argument of periapsis respectively. The drift rates due to only second order zonal harmonics (J_2) as given by Eq. (1.1c) and (1.1b) are used. A frozen inclination of either 63.4° or 116.6° is used so that $\dot{\omega}$ goes to zero. In order to create an axis of symmetry aligned with the Moon's spin axis, the argument of periapsis, ω, should be either 90° or 270°. These arguments of periapsis align the apse passages with the highest and lowest latitudes of the orbits.

Equation (1.6) can now be rearranged to solve for the nodal period, resulting in $T_\Omega = (N_\mathrm{d}/N_\mathrm{p})T_{\Omega_\mathrm{M}}$, where T_{Ω_M} is given by Eq. (1.5). This expression for the nodal period can then be substituted into Eq. (2.2), along with the secular drift terms given by Eq. (1.1), with a frozen orbit inclination so that $\dot{\omega} = 0$ rad/s, resulting Eq. (2.3a) [18].

$$T = \frac{2\pi}{\omega_\mathbb{C}} \frac{N_\mathrm{d}}{N_\mathrm{p}} \left(1 + 2\xi \frac{n}{\omega_\mathbb{C}} \cos i\right)^{-1} (1 + \xi\chi) \tag{2.3a}$$

$$\xi = \frac{3R_\mathbb{C}\ J_2}{4p^2} \tag{2.3b}$$

$$\chi = 4 + 2\sqrt{1 - e^2} - \left(5 + 3\sqrt{1 - e^2}\right) \tag{2.3c}$$

Finally, the two expressions for the anomalistic period given by Eqs. (2.1) and (2.3a) can be equated and used to solve for the semi-major axis, a. A numerical solver, such as MATLAB's built-in solver `vpasolve.m`, can be used to calculate a. From the semi-major axis, the eccentricity can be found, based on the design input for the radius of periapsis using the relationship $r_p = a(1 - e)$.

At this point, four of the six orbital elements for the flower constellation are known: i is set to a frozen inclination, a and e have been calculated, and ω is either 90° or 270°. The remaining orbital elements are the initial mean anomaly, M_0 and the RAAN, Ω, for each satellite.

2.1.2 Flower Constellation Phasing

The initial mean anomalies and the RAANs of the satellites in a flower constellation are determined using phasing schemes. The initial mean anomaly ($M_{k=1}(0)$) and RAAN ($\Omega_{k=1}$) for the first satellite in the constellation are designer inputs. The initial mean anomaly of the remaining satellites is determined based on the following mean anomaly phasing scheme [10]:

$$M_{k+1}(0) = M_k(0) + (\Omega_{k+1} - \Omega_k)\frac{N_\mathrm{p}}{N_\mathrm{d}} \tag{2.4}$$

Where $k = 1 : N_\mathrm{s}$. The phasing for the RAAN is used to create either a symmetric or an asymmetric constellation. For a symmetric constellation, the RAANs are distributed with equal spacing by Eq. (2.5) [11].

$$\Omega_{k+1} = \Omega_k - 2\pi\frac{N_\mathrm{d}}{N_\mathrm{s}} \tag{2.5}$$

While symmetric flower constellations are the more standard flower constellation, asymmetric flower constellations can actually be used to create formation flying schemes. Rather than evenly distributing the RAANs around the Moon, the satellites are placed into a specified RAAN range and bunched together to form a formation [11]. The phasing for an asymmetric flower constellation is based on the RAAN range input, $\Delta\Omega$, and is given by Eq. (2.6) [11].

$$\Omega_{k+1} = \Omega_k - \frac{\Delta\Omega}{N_\mathrm{s} - 1} \tag{2.6}$$

Previous work on flower constellations has used multiple orbit planes in either a symmetrical or asymmetrical RAAN distribution. Alternatively, a string-of-pearls (SOP) formation within just one orbit of a flower constellation can be created. This configuration is desirable due to the ease of deployment. In actual applications, a SOP formation may be used independently from other constellation satellites, or may occupy one orbit in an asymmetrical or symmetrical flower constellation. To distinguish these types of constellations, a flower constellation with multiple orbital planes will be called multi-petal and a constellation with only one inertial orbit will be called single-petal. The single-petal formation is set by placing the orbit at any desired RAAN

and then using the following mean anomaly phasing scheme to evenly distribute the satellites in a desired mean anomaly range ΔM:

$$M_{k+1}(0) = M_k(0) + \frac{\Delta M}{N_s - 1} \tag{2.7}$$

All orbital elements for a flower constellation have now been determined. The deployment scheme for a flower constellation at the Moon would be quite different than one at Earth. Additionally, flower constellations actually look quite distinct at the Moon compared to those at the Earth. The perturbations experienced at the Moon and Earth are also very dissimilar and significantly affect the lifetime of the constellation.

2.2 Flower Constellations at Earth

Flower constellations at the Earth are relatively simple. The dominant Earth perturbation is due to the oblateness of the Earth, given by J_2. Flower constellations are inherently designed to be J_2 compatible since the nodal period of the orbit is set to equal the nodal period of the Earth's rotation, given by Eq. (1.5) and Eq. (2.2) respectively. This accounts for the drift in the RAAN given by Eq. (1.1a). Flower constellations are also designed to be at a frozen inclination of either 63.4° or 116.6° so that the change in the argument of periapsis in Eq. (1.1b) is zero. There remains an unaccounted for drift in the mean anomaly, which is the only non-constant (for Keplerian motion) orbital element. The anomaly is already changing with time and all satellites in the constellation will drift in mean anomaly at the same rate with J_2 alone. Therefore, the perturbations from J_2 are all found to be acceptable and a long lifetime flower constellation at Earth can be achieved with minimal control efforts to maintain the geometry.

2.3 Flower Constellations at the Moon

2.3.1 Lunar Perturbations

Satellites at both the Earth and the Moon experience perturbations due to the non-sphericity of the central body, as well as third-body effects. However, the dominant Earth and lunar pertur-

bations are due to different sources and drastically affect the long-term evolution of orbits about them. At the Earth, the uniform J_2 through J_5 terms are the dominant source of perturbations[4]. The pertubations are also known as zonal harmonics and account for the oblateness of Earth. The J_2 perturbation is the strongest perturbation from the shape of the Earth, at nearly 1000 times larger than the next coefficient, J_3[16].

While the uniform J_2 through J_5 terms cause perturbations at the Moon, other significant perturbations cannot be neglected. Instead, orbits at the Moon are very affected by the irregular distribution of the mass of the Moon, as well as third-body effects from the Earth. The irregular mass distribution of the Moon is due to regions of high mass concentration, called mascons. The following breakdown describes the dominant lunar perturbations based on altitude[4]:

- Above $\sim$ 750 km: Third-body disturbances from Earth dominate
- Below $\sim$ 750 km: Mascons begin to influence orbits
- Below $\sim$ 100 km: Mascons dominate such that third-body effects can be neglected

The effects of these perturbations are highly dependent upon the geometry of the constellation and the Earth-Moon system at any given time. As the satellites pass over the surface of the Moon, the irregular gravity field will affect all satellites differently throughout their orbits. The effect of lunar mascons is also dependent on the current altitude of the satellite. The third body effect of the Moon will also greatly differ between orbits. Flower constellation orbits with a line of nodes aligned more with the Earth-Moon vector will be affected quite differently than orbits aligned more perpendicularly. When aligned parallel to the Earth-Moon vector, the gravitational pull of the Earth will act to raise either apoapsis or periapsis, depending on which apse is on the Earth side. Overall, the orbits will be elongated over time, increasing the semi-major axis and eccentricity. There will also be oscillations in the remaining orbital elements. Th Earth effects will less significantly impact those orbits aligned more perpendicularly with the Earth-Moon vector. The argument of periapsis and mean anomaly will rotate over time, with oscillations in the remaining

elements. Since all orbits at the Moon are affected in differing ways, the flower constellation symmetry will quickly break down.

As discussed in Chapter 1, due to the complex perturbations at the Moon, frozen orbits are very difficult to find. Frozen orbits that have been developed are for a specific set of orbital elements. However, as shown in Section 2.1, flower constellation satellites all have the same orbital elements with the exception of their mean anomaly and RAAN, making them unsuitable for existing frozen orbits schemes. Instead, the lunar perturbations will not be designed against, but rather included in simulations and corrected for with control schemes. The LP150q 50×50 lunar gravity model, as well as point mass influences from the Earth and Moon are included in numerical simulations of the flower constellations in Chapters 3 and 4.

The slow rotation period of the Moon versus that of the Earth also creates variations in flower constellations around the two bodies. The Moon rotation period is one sidereal day, whereas the Moon rotation period is on the order of a month, or 27.32 Earth days. For a one day repeat flower constellation ($N_\mathrm{p} = 1$), the semi-major axis and eccentricity grow incredibly large in order to produce orbits with periods of 27.32 Earth days. For a 5-1-4 constellation at the Moon, the semi-major axis would be 30,247 km ($17.4R_\mathrm{m}$) and the eccentricity is on the outer limits for an elliptical orbit at 0.9194. In contrast, a 5-1-4 constellation at Earth has a semi-major axis of only 14,446 km ($2.26R_\mathrm{e}$) and a reasonable eccentricity of 0.4893. The large semi-major axis and eccentricity required at the Moon for a $N_\mathrm{d} = 1$ flower constellation are actually prohibitively large. With a semi-major axis of nearly 8% of the Earth-Moon distance, the third body attraction of the Earth is so large that the satellites escape from the Moon. Without the effects of the Earth included, a 5-1-4 constellation is propagated at the Moon using GMAT software. The full 150x150 gravity field of the Moon is included, as well as third body effects from the Sun. The inertial and relative orbits produced are shown in Fig. 2.1. In Fig. 2.1, the orbits are maintained over time and produce a proper flower constellation, where the relative orbits all align, except for drift due to the Sun and lunar gravity field. However, once the third-body effects of the Earth are added, the orbits diverge and GMAT cannot even complete the integration. These orbits with Earth included

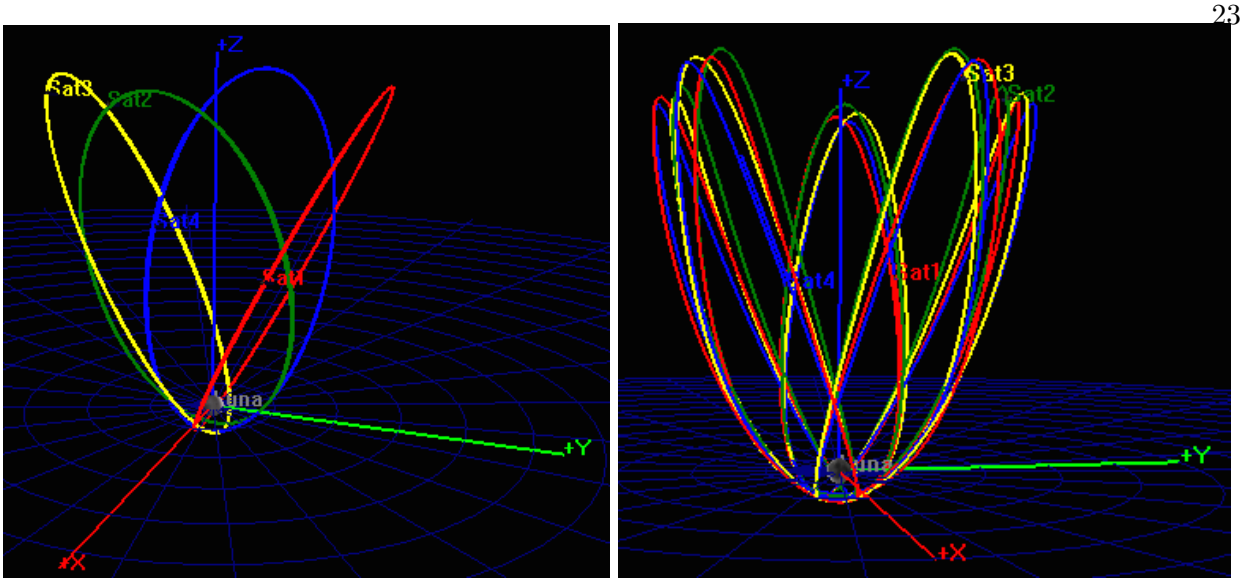

(a) Inertial orbits (b) Relative orbits

Figure 2.1: 5-1-4 FC at the Moon with no Earth effects

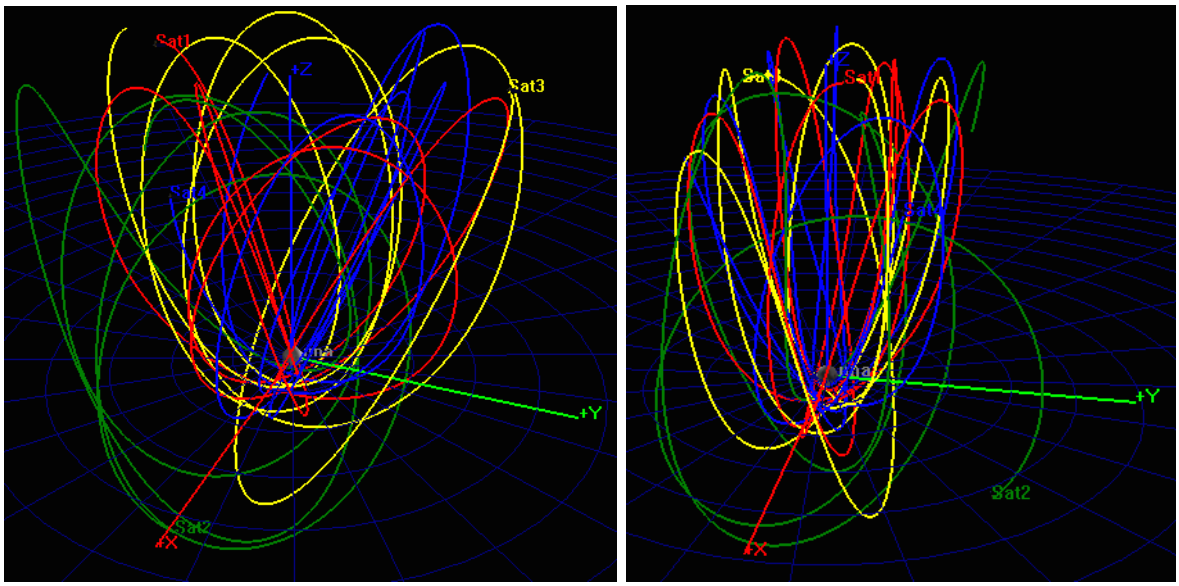

(a) Inertial orbits (b) Relative orbits

Figure 2.2: 5-1-4 FC at the Moon with Earth effects

are shown in Fig. 2.2. Clearly, constellations with semi-major axis and eccentricities of this scale are not feasible at the Moon. To remedy this problem, the period of the orbit, as given in Eq. (2.3a) must be decreased in order to reduce the size of the orbits. This can be achieved through the

scale factors N_p and N_d. Through decreasing N_d and/or increasing N_p, the period of repetition is decreased. In decreasing the nodal period, the anomalistic period also decreases, as shown by the relationship in Eq. (2.2). A smaller anomalistic period corresponds to a smaller semi-major axis, with the relationship of $a \propto T^{2/3}$ from Eq. (2.1). Since the radius of periapsis is a design input and remains constant once selected, a decrease in the semi-major axis corresponds to a decrease in the eccentricity through the equation $r_p = a(1-e)$.

The constellations produced by decreasing N_d to be less than one day have a different appearance than those created by increasing the number of petals, N_p. The result of decreasing N_d to be less than one day is shown in Fig. 2.3. The number of days to repeat is set to 1/10 of a day. When the height of periapsis is set to 250 km, this constellation has a semi-major axis of 6509 km and eccentricity of 0.69463.

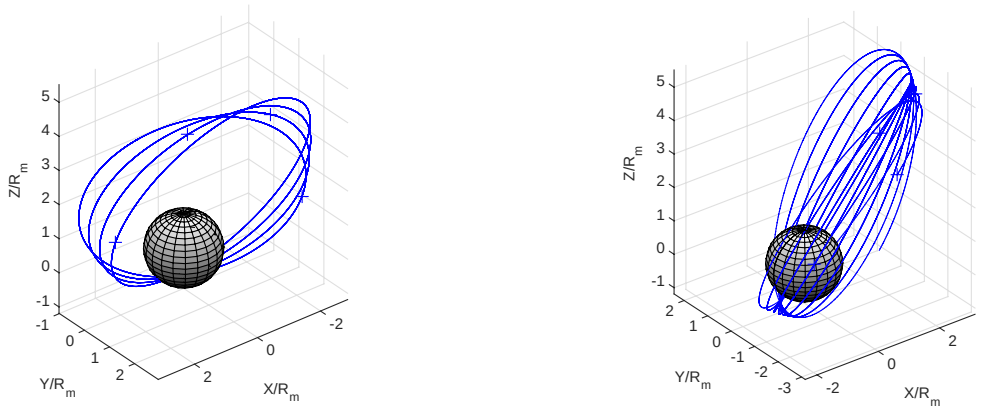

(a) Inertial orbits

(b) Relative orbits

Figure 2.3: 5-1/10-4 Flower constellation at the Moon

When $N_d = 1/10$ is put into Eq. (2.5), the resulting RAAN spacing actually becomes asymmetrical since the value of N_d/N_s is no longer an integer value. This can be visualized in Fig. 2.3a. However, the decreased repetition time does not actually correspond to the correct time to repeat, as seen by the incomplete relative orbits in Fig. 2.3b. In fact, the actual period to repeat is T_r calculated from Eq. (1.6) then divided by N_d when $N_d < 1$. Ultimately, this gives a constellation

with the same appearance of a flower constellation with $N_d = 1$, but the number of petals is actually N_p/N_d. Therefore, it is found that for the traditional flower constellation equations to remain true, N_d must be an integer value; additionally, the only effective way to decrease the nodal period of the orbit is to increase the number of petals, N_p. A 50 petal constellation is shown in Fig. 2.4 for comparison to Fig. 2.3. When the height of periapsis is set to 250 km, this constellation has a semi-major axis of 6509 km and eccentricity of 0.69463. These are the same semi-major axis and eccentricity as for $N_d = 1/10$. Both Fig. 2.3 and Fig. 2.4 were produced with J_2 as the only perturbation as the full perturbations at the Moon cause drifts in the orbits and will be discussed in Sections 3.3.3 and 4.2.3.

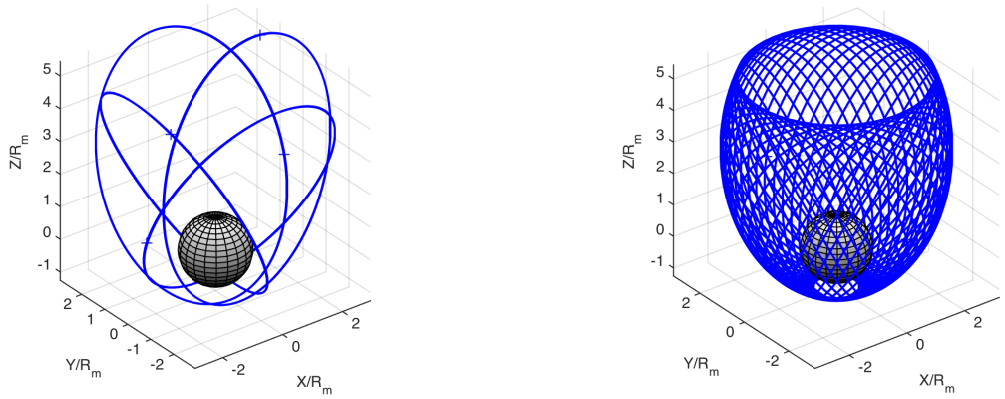

(a) Inertial orbits

(b) Relative orbits

Figure 2.4: 50-1-4 Flower constellation at the Moon

2.3.2 Vase Constellations

It should be noted that the slow rotation period of the Moon (27.32 Earth days) does significantly change the look (but not the fundamental principles) of flower constellations at the Moon compared to at Earth. In order to keep the semi-major axis and eccentricity of a lunar flower constellation orbit reasonable, it has been shown that the number of petals (N_p) must be large. At least 50 petals must be used to keep the eccentricity from nearing 1.0 and the semi-major axis small

enough that third body perturbations from the Earth are not dominant. This creates constellations that will look more like vases than flowers in the relative frame, as shown by Fig. 2.5. It can be seen in Fig. 2.6 that the inertial orbits are not significantly different, but due to the long rotation period of the Moon, the number of relative orbits increases.

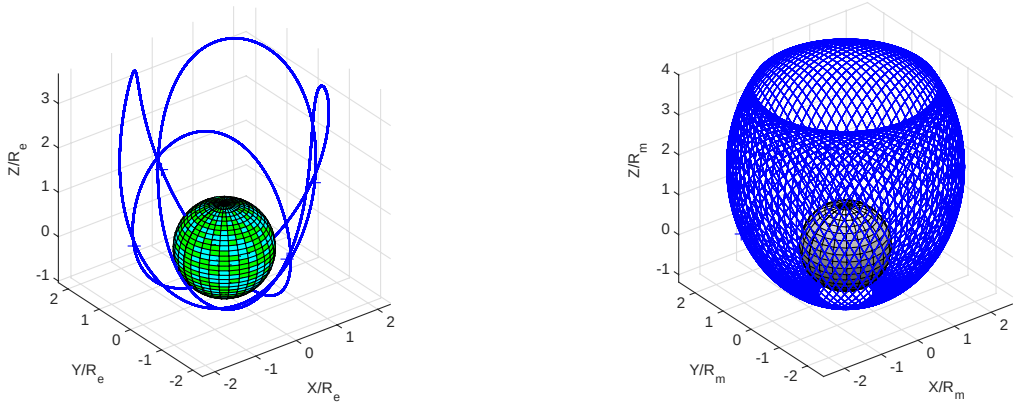

(a) 4-1-4 Flower constellation at Earth (b) 73-1-4 Flower constellation at the Moon

Figure 2.5: Flower constellation relative orbits at Earth and the Moon

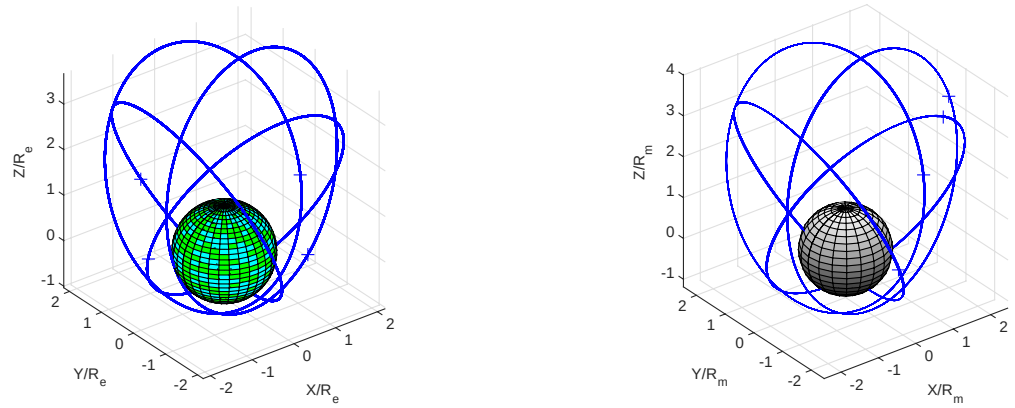

(a) 4-1-4 Flower constellation at Earth (b) 73-1-4 Flower constellation at the Moon

Figure 2.6: Flower constellation inertial orbits at Earth and the Moon

The new look of flower constellations at the Moon creates so many petals that they become

difficult to distinguish from one another. The term vase is perhaps more appropriate to describe the look of the constellations in the relative frame now. It is also interesting to compare the vase constellation in Fig. 2.5b to the 73-cycle to repeat RGT orbits of Fig. 1.2a. In fact, the repeat ground track orbits created in Reference 12 are simply flower constellations with 73 and 328 petals, so that they appear as vase constellations in the relative frame.

2.3.3 Design Tradeoffs

Repeat ground track orbits at the Moon have been found in Reference 12. These orbits were found to have a long lifetime. However, these were still only approximations as the lp150q gravity field and the Earth-Moon RTBP were used. Because these RGT orbits are both approximate, albeit high level, methods, they would not hold up in a truly arbitrary lunar gravity field or under the actual third body effects from the Earth. Control laws and station-keeping are required with these orbits, although the extent of the control ΔV is likely to be minimized through the efforts to find orbits that work well with the natural dynamics around the Moon. Likewise, general lunar frozen orbits have also been found, but these will also require station-keeping as they are also just approximations.

Ultimately, the frozen orbits of References 3, 4, and 12 are not practical for use in a flower constellation at the Moon. These orbits obtain frozen properties through a unique combination of the six orbital elements. In a flower constellation, the orbit elements are not free to be chosen at random since they must satisfy the repeat ground track and phasing requirements. The semi-major axis and eccentricity are dependent upon one another and are tied to the rotation period of the Moon and the parameters N_d and N_p. The argument of periapsis is designed to be either 90° or 270° in order to orient apoapsis at either the lowest or highest point in the constellation respectively. The RAAN spacing is dependent upon the constellation shape desired and the phasing scheme given in Eq. (2.5) and Eq. (2.6). The inclination is desired to be a frozen inclination, which is achieved by solving the analytical expressions for the second-order secular drift rates given by Eq. (1.1). However, if an alternative frozen inclination were to be found at the Moon that was independent

of all other orbit parameters, this inclination would be used instead. Unfortunately, that has not been shown to exist. Therefore, there is no feasible way to establish a flower constellation at the Moon that fully utilizes the frozen orbit properties of References 4, 3, and 12. Additionally, even these frozen orbits are still approximations that would require station-keeping over time.

In order to achieve a flower constellation at the Moon, a true frozen orbit is sacrificed, requiring station-keeping. Therefore, approximations using only second-order zonal harmonics are still used in designing flower constellations at the Moon, just as they were used at Earth. The effects of lunar mascons and third body effects vary based on the satellite altitude and location over the lunar surface and are, therefore, not feasible to include in designing a flower constellation. Stationkeeping through the use of impulsive control laws will be required to maintain the flower constellation formation over time.

Chapter 3

Single-Petal Flower Constellations

Flower constellations typically include three or more orbits, distributed with either a symmetrical or asymmetrical RAAN distribution, according to Eq. (2.5) or Eq. (2.6) respectively. However, in this section, a special case, where a string-of-pearls formation is created within a single flower constellation orbit is studied. This is referred to as a single-petal flower constellation due to the nature of the single inertial orbit used. In order to match the repeat ground tracks of Russell in Reference 12, a 73-1-4 constellation is studied, with a height of periapsis of 250 km is used throughout this chapter.

3.1 Deployment Scheme

The flower constellation studied is a 73-1-4 constellation with a height of periapsis of 250 km. The four satellites are placed in a string-of-pearls formation (i.e., the only orbital element difference is in mean anomaly). A mean anomaly range, ΔM, of 21° is chosen and the phasing scheme given by Eq. (2.7) is used. A RAAN of 0° and mean anomaly of the first satellite of 0° are chosen. The initial desired orbit elements of the constellation satellites are given in Table 3.1.

Table 3.1: Orbital Elements for Flower Constellation Satellites

Satellite	a (km)	e	i (deg)	ω (deg)	Ω (deg)	M_0 (deg)
1	5053.73	0.60670	63.4	270	0	0
2	5053.72	0.60670	63.4	270	0	7
3	5053.72	0.60670	63.4	270	0	14
4	5053.72	0.60670	63.4	270	0	21

The deployment of a string of pearls constellation is achieved by placing the mothercraft in an orbit with a different semi-major axis, and, thus, different period from the desired flower constellation orbit. The difference in period between the two orbits is based on the desired mean anomaly separation between each satellite ($\delta M = \Delta M/(N_{\mathrm{p}} - 1)$), which for this scenario, is 7°. This deployment scheme is illustrated in Fig. 3.1.

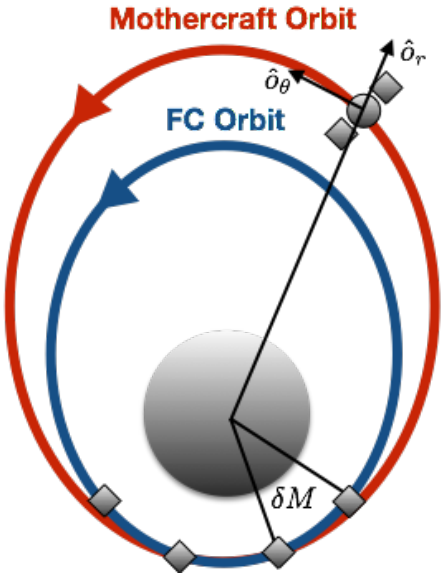

Figure 3.1: Deployment scheme for single-petal FC

A factor, K, is also used to determine how many orbits the mothercraft will complete between deploying sequential satellites. Equation (3.1) shows the relationship between the mothercraft period (T_{MC}) and the period of the flower constellation orbit (T_{FC}).

$$T_{MC} = T_{\mathrm{FC}} + \frac{\delta M}{n_{\mathrm{FC}} K} \tag{3.1}$$

Where N_{FC} is the mean motion of the flower constellation orbit. Through increasing K, the semi-major axis difference can be decreased, which decreases the relative velocity between the mothercraft and flower constellation orbits. Reducing this relative speed decreases the deployment speed required as the flower constellation satellites are released and put into their proper orbit slots. A small semi-major axis difference is desired as the impulsive ΔV that matches the small satellites to the flower constellation orbits will be entirely achieved by the cubesat deployment system on

the mothercraft. The poly picosatellite orbital deployer (P-POD) is a standard deployment system and will be used as a baseline for the attainable ΔV in the cubesat deployment. The nominal rates of deployment for the P-POD have been shown to be 1.6-2 m/s[7]. For this study, a rate of up to 2 m/s is assumed to be achievable.

Once the mothercraft period has been determined, the semi-major axis can be solved for using the standard period expression given in Eq. (2.1). The radius of periapsis is set to the same radius of periapsis of the flower constellation orbit, which was a user input in the flower constellation design. From the radius of periapsis and semi-major axis of the mothercraft deployment orbit, the eccentricity can be solved for using the expression from orbital mechanics of $r_{\mathrm{p}} = a(1-e)$, where r_{p} is the radius of periapsis. The deployment is then implemented by releasing a satellite at every K^{th} periapsis passage of the mothercraft. The required ΔV at which the flower constellation cubesats must be released is determined by the difference in the mothercraft and flower constellation orbit velocities at periapsis. The well-known vis-viva equation is useful to solve for the velocity at periapsis of both mothercraft orbit and the flower constellation orbit, as given in Eq. (3.2)[16]. The impulsive ΔV required is the difference between these two periapsis velocities. This process continues until all desired satellites have been deployed.

$$v = \sqrt{\frac{2\mu}{r} - \frac{\mu}{a}} \tag{3.2}$$

After deployment is complete, the mothercraft must maneuver from the deployment orbit to the longterm communications orbit. The longterm communications orbit creates a relative orbit that is designed to orbit the flower constellation orbit element barycenter (FC barycenter). The orbit element barycenter is calculated by finding the average of the flower constellation satellite elements. The simple average, rather than the weighted average, can be used under the assumption that all flower constellation satellites are identical and have the same mass.

The goal of the longterm mothercraft communications orbit is to remain close enough to all the flower constellation satellites for communications purposes. The flower constellation satellites themselves are likely to have limited communications ranges due to the simplicity of cubesat

hardware. The flower constellation satellites will, therefore, communicate over a short range to the mothercraft; the mothercraft will then be responsible for all communication with Earth. The desired communications orbit for the mothercraft will have the same orbit elements as the FC barycenter, with only an eccentricity difference. An eccentricity difference in formation flying creates a 2:1 ellipse of the deputy (mothercraft) about the chief (FC barycenter). At the end of deployment, the mothercraft will have a difference in a, e, and M from the FC barycenter. The semi-major axis and eccentricity differences are typically small, due to the factor K that dictates that the mothercraft complete multiple orbits between sequential deployments. Since the differences are small, they could potentially be corrected with the impulsive orbit element control that will be used to maintain the constellation. However, the mean anomaly difference from the barycenter at the end of deployment will be half of the prescribed string-of-pearls mean anomaly range, ΔM. For this study, that is over 10°, which is considered too large for the impulsive orbit element control method. Instead, a two-burn mean anomaly correction is performed to maneuver the mother craft into the communications orbit.

The first burn of the two-impulse mean anomaly correction is set to occur at the first periapsis passage after the final flower constellation satellite deployment at periapsis. This maneuver places the mothercraft in a phase orbit that will correct the mean anomaly error. This first burn alters the semi-major axis, eccentricity, and radius of apoapsis of the mothercraft. Based on the desired phase orbit, the semi-major axis, and the initial radius of periapsis, the radius of apoapsis and the eccentricity will change according to Eq. (3.3).

$$r_{\mathrm{p}} = a(1 - e) \tag{3.3a}$$

$$r_{\mathrm{a}} = a(1 + e) \tag{3.3b}$$

It is recalled that in the final mothercraft orbit, only an eccentricity difference is desired from the flower constellation satellites. For an orbit to have the same semi-major axis as another orbit, but a different eccentricity, the radii of periapsis and apoapsis must both be shifted. The

first burn will have already shifted the radius of apoapsis, which can contribute to an eccentricity difference in the final mothercraft orbit. Therefore, the second burn is desired to occur at apoapsis in order to maintain the shifted radius of apoapsis while still matching the desired semi-major axis, as determined by the flower constellation satellites. This burn will, therefore, shift the radius of periapsis. Since the first burn occurs at periapsis and the second at apoapsis, the mean anomaly correction will occur over 1.5 phase orbits. In other words, 2/3 of the mean anomaly error is corrected in one phase orbit period and the remaining 1/3 is corrected in the final half-phase orbit period. The phase orbit is designed so that the mothercraft periapsis is raised to an orbit that has a period equal to the flower constellation orbit period, plus the time needed to cover 2/3 of the mean anomaly difference. This is described by Eq. (3.4), where ϕ is the phase angle between the mothercraft and the FC barycenter. In other words, ϕ is the initial mean anomaly error. In this study, ϕ is a negative value (desired minus actual), and the phase orbit will have a smaller semi-major axis, and therefore, shorter period, than the flower constellation orbit.

$$T_{\text{phase}} = \frac{2\pi + \frac{2\phi}{3}}{n_{\text{FC}}} \tag{3.4}$$

As was done with the deployment orbit and Eq. (3.1), from Eq. (3.4), the phase orbit semi-major axis can be determined as shown in Eq. (3.5a). From there, the vis-viva equation given in Eq. (3.2) can be used to find the velocity of the mothercraft at periapsis in the original deployment orbit ($V_{\text{p,deploy}}$) and the velocity at periapsis required for the phasing orbit ($V_{\text{p,phase}}$). These expressions are given in Eq. (3.5b) and (3.5c) respectively. The difference in these velocity magnitudes is the impulsive ΔV_1 required to place the mothercraft into the phasing orbit, with the

burn applied in the along-track direction.

$$a_{\text{phase}} = \left[\mu\left(\frac{6\pi + 2\phi}{6\pi n_{\text{FC}}}\right)^2\right]^{1/3} \tag{3.5a}$$

$$V_{\text{p,deploy}} = \sqrt{\frac{2\mu}{r_{\text{p,deploy}}} - \frac{\mu}{a_{\text{deploy}}}} \tag{3.5b}$$

$$V_{\text{p,phase}} = \sqrt{\frac{2\mu}{r_{\text{p,deploy}}} - \frac{\mu}{a_{\text{phase}}}} \tag{3.5c}$$

$$\Delta V_1 = V_{\text{p,phase}} - V_{\text{p,deploy}} \tag{3.5d}$$

After 1.5 phasing orbits have been completed, the mothercraft makes a second burn at apoapsis (ΔV_2) to match the desired flower constellation semi-major axis. Again, the vis-viva equation is used to find the magnitude of this burn, using the radius of apoapsis of the phase orbit and the semi-major axis of the phase orbit and the desired orbit to find the initial and final velocities at apoapsis respectively. These velocity magnitudes are given by Eq. (3.6a) and (3.6b). This burn is also in the along-track direction; once completed, the mothercraft will be in the desired long-term orbit with only an eccentricity difference from the flower constellation barycenter.

$$V_{\text{a,phase}} = \sqrt{\frac{2\mu}{r_{\text{a,phase}}} - \frac{\mu}{a_{\text{phase}}}} \tag{3.6a}$$

$$V_{\text{a,final}} = \sqrt{\frac{2\mu}{r_{\text{a,phase}}} - \frac{\mu}{a_{\text{FC}}}} \tag{3.6b}$$

$$\Delta V_2 = V_{\text{a,final}} - V_{\text{a,phase}} \tag{3.6c}$$

This final eccentricity difference is dependent on the phase angle, ϕ, which is dependent upon the desired number of satellites, N_{s}, and the mean anomaly range, ΔM. Since there is no strict requirement on the eccentricity difference, only the requirement that there be an eccentricity difference, this variability is found to be acceptable.

3.2 Impulsive Orbit Element Control

Many control laws utilize continuous thrust methods. However, impulsive control laws can be used to correct errors at specific times in an orbit, rather than correcting continually. The presented control laws correct upon orbit element errors rather than position and velocity. They are intended for use with mean orbit elements, rather than correcting on osculating errors. Specifically, considering only J_2, a, e, and i are constant in the mean sense, but do experience osculating perturbations. Conversely, Ω, ω, and M vary secularly over time. Therefore, it is desirable to correct the mean elements, rather than correcting on osculating errors that do not exist over time. There also exists a first-order mapping between osculating and mean elements developed by Brouwer[2] and Lyddane[8]. However, at the Moon, J_2 is not as strongly dominant, deeming this first order mapping is insufficient. Additionally, the Brouwer-Lyddane mapping breaks down due to a singularity at frozen inclinations. Therefore, for the purposes of this investigation, osculating elements will be used in the impulsive orbit element control law, recognizing that some increase in the calculated fuel costs may result.

The orbit element vector is defined as $\boldsymbol{oe} = (a, e, i, \Omega, \omega, M)$, with all angle values in radians. The orbit element error vector that the impulsive control law feedbacks on is the difference in the desired orbit elements ($\boldsymbol{oe}_{\mathrm{d}}$) and the actual orbit elements of the deputy ($\boldsymbol{oe}_{\mathrm{d}}$):

$$\Delta\boldsymbol{oe} = \boldsymbol{oe}_{\mathrm{d}} - \boldsymbol{oe}_{\mathrm{a}} \tag{3.7}$$

The impulsive feedback control law developed in Reference 14 presents this control method based on Gauss's variational equations of motion. Gauss's variational equations of motion describe the rate of change of orbital elements based on disturbance (i.e. non-Keplerian) perturbations[16]. Gauss's variational equations expressed in terms of acceleration components ($\hat{a}_{\mathrm{r}}$, $\hat{a}_{\theta}$, and $\hat{a}_{\mathrm{h}}$) in

local vertical/local horizontal (LVLH) frame components is given by Eq. (3.8).

$$\frac{\mathrm{d}a}{\mathrm{d}t} = \frac{2a^2}{h}\left(e\sin f\ a_{\mathrm{r}} + \frac{p}{r}a_\theta\right) \tag{3.8a}$$

$$\frac{\mathrm{d}e}{\mathrm{d}t} = \frac{1}{h}\left(p\sin f\ a_{\mathrm{r}} + \left((p+r)\cos f + re\right)a_\theta\right) \tag{3.8b}$$

$$\frac{\mathrm{d}i}{d\mathrm{d}} = \frac{r\cos\theta}{h}a_h \tag{3.8c}$$

$$\frac{\mathrm{d}\Omega}{\mathrm{d}t} = \frac{r\sin\theta}{h\sin i}a_h \tag{3.8d}$$

$$\frac{\mathrm{d}\omega}{\mathrm{d}t} = \frac{1}{he}\left(-p\cos f\ a_{\mathrm{r}} + (p+r)\sin f\ a_\theta\right) - \frac{r\sin\theta\cos i}{h\sin i}a_h \tag{3.8e}$$

$$\frac{\mathrm{d}M}{\mathrm{d}t} = n + \frac{\eta}{he}\left(\left(p\cos f - 2re\right)a_{\mathrm{r}} - (p+r)\sin f\ a_\theta\right) \tag{3.8f}$$

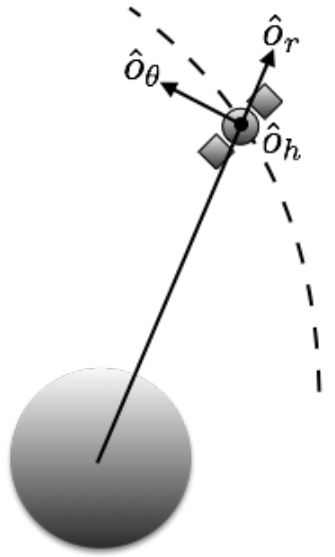

Figure 3.2: LVLH coordinate frame

Where f is the true anomaly, p is the semi-latus rectum, and h is the angular momentum magnitude. It should also be noted that η and the true latitude, θ, are non-singular expressions for

the eccentricity and true anomaly respectively:

$$\eta = \sqrt{1 - e^2} \tag{3.9a}$$

$$\theta = f + M \tag{3.9b}$$

It is important to note that the control accelerations in Eq. (3.8) are in the local vertical/local horizontal (LVLH) frame. The LVLH frame is a rotating reference frame located at the center of mass of a satellite. Figure 3.2 illustrates the LVLH frame centered on a body with a satellite located at a relative position $\boldsymbol{\rho}$ from the origin. The three axis of the LVLH frame are the radial ($\hat{o}_\mathrm{r}$), along-track ($\hat{o}_\theta$), and out of plane ($\hat{o}_\mathrm{h}$) directions.

From Gauss's variational equations, insight can be gained as to how control thrusts will affect individual orbital elements. For example, it can be seen that the inclination and RAAN are only affected by disturbances in the out-of-plane, $\hat{o}_\mathrm{h}$-direction[13]. From Eq. (3.8), it can be determined when it is most efficient to make individual element corrections. From the insight gathered from Gauss's variational equations, nearly optimal impulsive feedback control laws were developed in Reference 5. Corrections are applied impulsively at points in the orbit where the effect on the orbit element to be corrected is greatest. The control is also applied in directions that cause as little impact on the other elements as possible. The control scheme for correcting inclination and RAAN are performed as a pair since they are both only dependent on out-of-plane accelerations[14]:

$$\theta_c = \arctan \frac{\Delta\Omega \sin i}{\Delta i} \tag{3.10a}$$

$$\Delta v_\mathrm{h} = \frac{h}{r}\sqrt{\Delta i^2 \Delta\Omega^2 \sin^2 i} \tag{3.10b}$$

$$\Delta i = \frac{r \cos\theta_\mathrm{c}}{h} \Delta v_\mathrm{h} \tag{3.10c}$$

$$\Delta\Omega = \frac{r \sin\theta_\mathrm{c}}{h \sin i} \Delta v_\mathrm{h} \tag{3.10d}$$

To implement this correction series, the optimal true latitude given in Eq. (3.10a) must first be calculated. This true latitude is where the impulsive Δv_h will create the largest change in

the inclination and RAAN. There will always be two critical angles that satisfy Eq. (3.10a), but for this control strategy, only the positive angle– corresponding to the positive Δv_{h} given by Eq. (3.10b)–is used[14]. The magnitude of the burn is dependent upon the magnitude of the errors to be corrected. The changes in inclination and RAAN that will result from the impulsive burn are shown by Eq. (3.10c) and (3.10d). It can be seen from Eq. (3.8e) that the argument of periapsis also has a dependence on a_{h}. By correcting the inclination and RAAN, the argument of periapsis will also be affected, as a function of the RAAN correction made[14]:

$$\Delta\omega(\Delta v_{\mathrm{h}}) = -\cos i \Delta\Omega \tag{3.11}$$

Like the inclination and RAAN, the argument of periapsis and mean anomaly are also corrected as a pair since both parameters correspond to the position of the satellite within the orbital plane. These burns will also account for the change in ω created by correcting the inclination and RAAN, as given in Eq. (3.11). The burns for these corrections are split so as to be performed at periapsis and apoapsis in the radial direction[14]:

$$\Delta v_{\mathrm{r_p}} = -\frac{na}{4}\left(\frac{(1+e)^2}{\eta}\left(\Delta\omega + \Delta\Omega\cos i\right) + \Delta M\right) \tag{3.12a}$$

$$\Delta v_{\mathrm{r_a}} = -\frac{na}{4}\left(\frac{(1-e)^2}{\eta}\left(\Delta\omega + \Delta\Omega\cos i\right) + \Delta M\right) \tag{3.12b}$$

The remaining elements to be corrected are the semi-major axis and eccentricity. These elements are also corrected as a pair since both control the size and shape of the orbit. The burns for these corrections are also split to be performed at periapsis and apoapsis, but in the along-track direction[14]:

$$\Delta v_{\theta_{\mathrm{p}}} = \frac{na\eta}{4}\left(\frac{\Delta a}{a} + \frac{\Delta e}{1+e}\right) \tag{3.13a}$$

$$\Delta v_{\theta_{\mathrm{a}}} = \frac{na\eta}{4}\left(\frac{\Delta a}{a} - \frac{\Delta e}{1-e}\right) \tag{3.13b}$$

The implementation of this control law involves calculating the orbit element errors at one point in the orbit, then controlling based off these errors for the remainder of the orbit. Corrections will be performed once at each θ_c, periapsis, and apoapsis passage, for a total of three burns per orbit. After an orbit is completed, the errors are updated for the corrections in the next orbit.

3.3 Numerical Simulation

The simulation of a single-petal flower constellation is broken into three mission portions: deployment, mothercraft maneuver, and longterm orbit maintenance. The simulations of this chapter, as well as Section 4.2 utilize original MATLAB code as well as the publicly available `lprop.m` MATLAB script for predicting the evolution of lunar orbits, written by David Eagle. The code utilizes the LP150q 50×50 lunar gravity model, as well as point mass influences from the Earth and Moon.

3.3.1 Deployment

The deployment simulation does not include any perturbations. It is important to note that in real applications, the irregular gravity field of the Moon and third-body effects from the Sun and Earth would need to be considered. Instead, this simulation assumes that any initial errors that would result from ignoring perturbations can be corrected for through the controls in the first long-term orbit maintenance maneuver.

In the deployment phase, it is desired for the flower constellation satellites to be placed in the orbit slots given in Table 3.1. This is implemented using the method described in Section 3.1, with $K = 5$ in Eq. (3.1). The value of $K = 5$ is selected in order to bring the impulsive ΔV required for deployment down to within the 2 m/s limit capable by the cubesat deployment system. The ΔV magnitude required when $K = 5$ is actually 0.550680 m/s. This is well within the capability of a cubesat deployer. A larger value of K could be used, but as the long-term mothercraft orbit is desired to have the same semi-major axis as the flower constellation orbit, K is set to five in order to reduce the cost of maneuvering the mothercraft into its final orbit after deployment. The

orbital elements achieved at the end of the deployment phase for the flower constellation satellites are shown in Table 3.2. In comparison to the elements in Table 3.1, it can be seen that the desired elements are achieved with just small errors in the initial mean anomalies. These errors can be corrected for in the first long-term orbit maintenance maneuver.

Table 3.2: Orbital elements for flower constellation satellites after deployment

Satellite	a (km)	e	i (deg)	ω (deg)	Ω (deg)	M_0 (deg)
1	5053.73	0.60670	63.4	270	0	-0.4275
2	5053.72	0.60670	63.4	270	0	6.5722
3	5053.72	0.60670	63.4	270	0	13.5725
4	5053.72	0.60670	63.4	270	0	20.5729

The inertial orbits at the end of the deployment phase are shown in Fig. 3.3. The red orbit is the orbit of the mothercraft and the blue orbit is the flower constellation orbit. In this view, the two orbits appear to be the same, but there are small differences in semi-major axis and eccentricity, as shown in Table 3.3. The red circle indicates the mothercraft's location at the final deployment and the blue plus signs represent the flower constellation satellites. The final flower constellation satellite and the mothercraft satellites are shown to be at the same location at the moment of deployment.

Table 3.3: FC and mothercraft orbits during deployment

Orbit	a (km)	e	i (deg)	ω (deg)	Ω (deg)
Flower Constellation	5053.73	0.60670	63.4	270.0	0
Mothercraft	5066.82	0.60771	63.40	270.0	0

Now that the deployment phase has been completed, the large mean anomaly difference between the mothercraft and the flower constellation barycenter must be corrected.

3.3.2 Mothercraft Orbit Maneuver

Now that deployment of the flower constellations satellites is complete, the mothercraft must move into its long-term communications orbit. At the end of the deployment phase, the initial mean

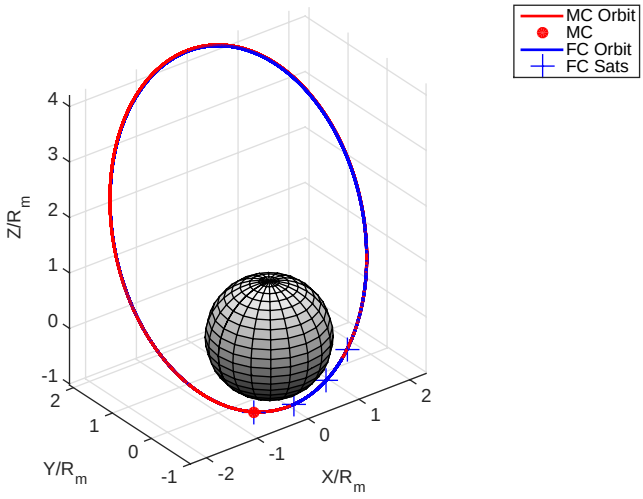

Figure 3.3: Inertial Orbits at moment of final FC satellite deployment

anomaly error is $-11.90°$ for this study. This is too large of a correction for the impulsive orbit element control presented in Section 3.2. Instead, this correction is made as two impulsive burns, as described in Section 3.3.2 and Eq. (3.4). The inertial orbits during the mean anomaly correction period are shown in Fig. 3.4. The first burn has a magnitude of 4.2794 m/s and the second burn has a magnitude of 14.4396 m/s, both in the along-track direction. These burn magnitudes are small and found to be acceptable.

In Fig. 3.4a, the mothercraft starts at periapsis on the black orbit. The black dot shows where the first maneuver is made at periapsis to lower the mothercraft into the phase orbit shown in red. The phase orbit elements are given in Table 3.4. After 1.5 phase orbits, the second maneuver is made at apoapsis, marked by the red dot. The resulting orbit is the final mothercraft orbit shown in blue in Fig. 3.4a. This new mothercraft orbit is also given in Table 3.5 and matches the flower constellation orbit but with an eccentricity difference. The mothercraft orbits during this correction period are shown with the flower constellation orbit in Fig. 3.4b. The final position of the mothercraft relative to the flower constellation satellites can be seen; as desired, the mothercraft is aligned with the mean anomaly of the flower constellation barycenter.

The initial and final flower constellation and mothercraft orbit elements, as well as the phase

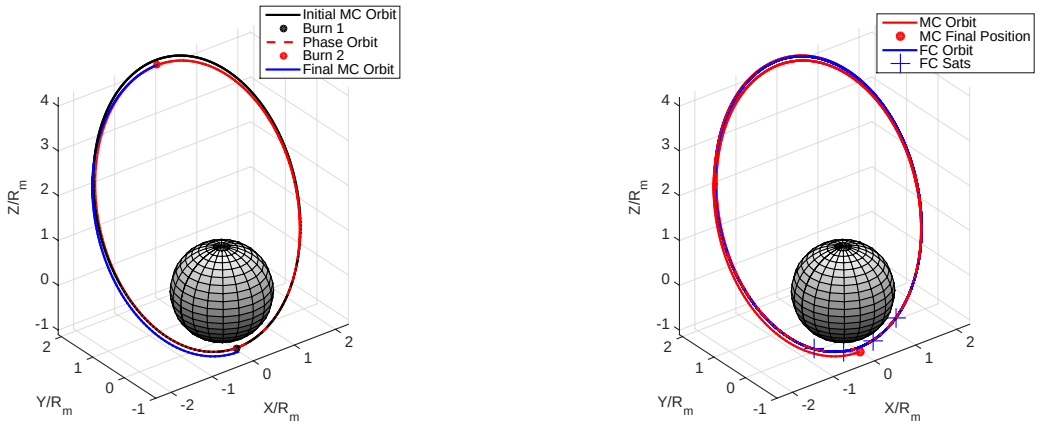

(a) Mothercraft Mean Anomaly Phase Orbit (b) Inertial Orbits at end of mean anomaly correction

Figure 3.4: Mothercraft mean anomaly correction

orbit elements are given in Table 3.5. All mothercraft orbit values in Table 3.5 are taken at apoapsis, as this is where the final maneuver occurs

It can be seen from Table 3.5 that at the end of the mean anomaly correction phase of the mission, the mothercraft orbit elements nearly match those of the FC barycenter. The most significant element difference is in the eccentricity, but an eccentricity difference is desired in order to create the closed relative orbit of the mothercraft about the FC barycenter for communications purposes. At this point, all remaining orbit element errors are small enough to be corrected using the impulsive orbit element control law.

3.3.3 Long-Term Orbit Maintenance

Once the constellation has been deployed, the flower constellation satellites will be subject to the various perturbations at the Moon. These perturbations include the 50×50 lunar gravity field as well as the third-body effects from the Sun and Earth. Flower constellation satellites are designed to be J_2 compatible. This means that they are intended to drift from perturbations caused by the oblateness of their central body. Flower constellations are at frozen inclinations in a second-order zonal sense so the argument of periapsis does not change due to J_2. The drift in the RAAN

Table 3.4: Phase orbit elements

	a (km)	e	i (deg)	ω (deg)	Ω (deg)
Phase Orbit	4979.21	0.60081	63.40	270.00	0

is accounted for when determining the nodal period, and any drift in the mean anomaly does not affect the repeat ground-track nature of the constellation. However, at the Moon, J_2 is not the dominant perturbation it is at Earth. In fact, higher order zonal and tesseral terms are nearly the same order of magnitude as J_2 and, therefore, cannot be ignored. Additionally, the Sun and Moon cause large periodic variations in the orbital elements. As was discussed in the literature review, true frozen orbits at the Moon are difficult to find and are not useful for this application. Instead, a J_2 frozen inclination of 63.4° is used and impulsive corrections will be needed to maintain the desired flower constellation orbital elements over time.

The impulsive orbit element controls presented in Section 3.2 are used to correct orbital elements to their desired values. The errors in the orbital elements are found by subtracting the actual element values from the desired element values. The desired elements are as given in Table 3.6: The semi-major axis, eccentricity, and inclination are desired to remain constant since they have constant mean values under J_2 alone. The argument of periapsis should also be constant as the J_2 frozen inclination eliminates the drift, $\dot{\omega}$ given by Eq. (1.1b). However, the RAAN and mean anomaly will change with J_2, and as this is desired in a flower constellation, these drifts will not be controlled against. The drift in RAAN, $\dot{\Omega}$, is given by Eq. (1.1a) and the drift in initial mean anomaly, $\dot{M}_0$, is given by Eq. (1.1c). The term Δt is simply the elapsed time since the initial time, t_0, and n_d is the desired mean motion, calculated using the desired semi-major axis, a_d. The

Table 3.5: Orbits during mean anomaly correction

Orbit	a (km)	e	i (deg)	ω (deg)	Ω (deg)	M (deg)
Initial FC Barycenter	5053.73	0.60670	63.40	270.00	0	11.8754
Initial MC	5066.82	0.60772	63.40	270.00	0	360.9996
Final FC Barycenter	5053.73	0.60670	63.40	270.00	0	359.8478
Final MC	5053.73	0.57721	63.40	269.98	359.80	359.8455

Table 3.6: Desired Elements for a 73-1-4 FC

Element	Desired Value
a_{d} (km)	a_0
e_{d}	e_0
i_{d} (deg)	i_0
ω_{d} (deg)	w_0
Ω_{d} (deg)	$\Omega_0 + \dot{\Omega}\Delta t$
M_{d} (deg)	$M_0 + (n_{\mathrm{d}} + \dot{M}_0)\Delta t$

values for the initial orbit elements can be found in Table 3.1.

Small cube satellites are assumed for the flower constellation satellites. Since fuel is limited, the accuracy of the flower constellation orbits must be sacrificed. To maintain the desired orbit elements at all times would severely limit the lifetime of the constellation. Instead, it is proposed that the orbits be corrected every four days over one repetition period (T_{r}) for the constellation. Recall that the repetition period is the value T_{r} as given by Eq. (1.6) with N_{d} set to one lunar day, or approximately 27 Earth days. Each control phase allows for the controls to act over five orbits. A two minutes time step is used for the propagation.

3.3.3.1 Control Simulation Results

The relative orbits for the repetition period and for the control orbits are shown in Fig. 3.5a. The overall vase shape is maintained although the perfect latticework of the relative orbits is somewhat compromised by the lunar perturbations. This is most obvious in the back portion of Fig. 3.5, where the constellation begins to repeat itself.

The inertial orbits over the repetition period and control phase are shown in Fig. 3.6. It can be seen that the perturbations cause drift in the inertial orbits over the 27-day repetition period.

The control costs for one repetition period for each satellite are shown in Table 3.7. The highest control cost is for satellite one, whereas the lowest control cost is for satellite four. Since all satellites are in the same orbit, they should all behave similarly under the effects of the perturbations and under the impulsive orbit element controls. However, the implementation of the

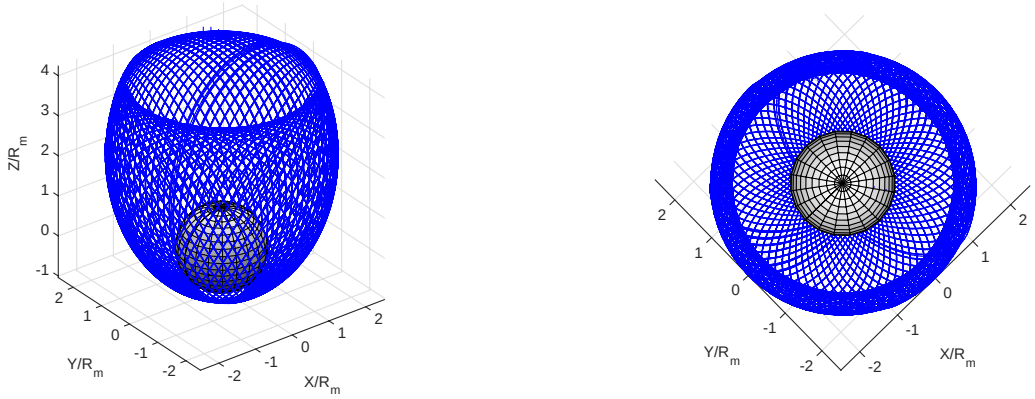

(a) Isometric view (b) Polar view

Figure 3.5: 73-1-4 single-petal FC relative orbits

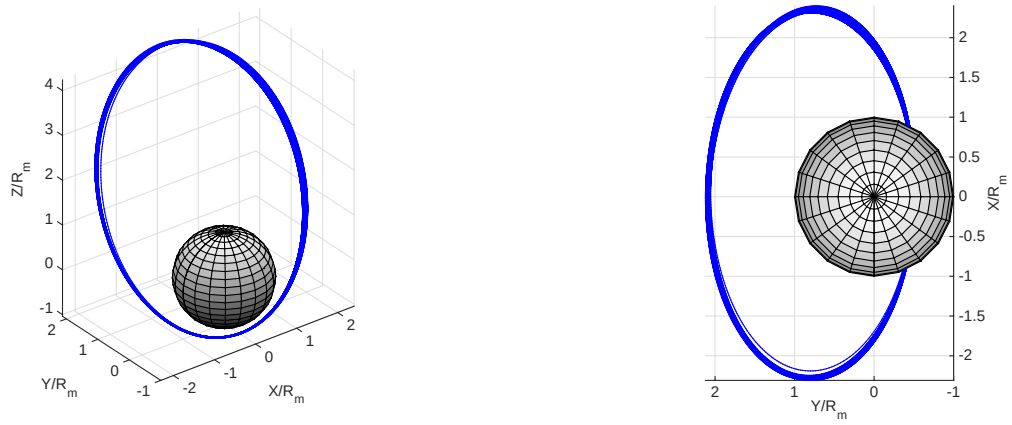

(a) Isometric view (b) Polar view

Figure 3.6: 73-1-4 single-petal FC inertial orbits

control laws is sensitive to the integration time step used. As was discussed in Section 3.2, in-plane element corrections are to be applied at apoapsis and periapsis, whereas out-of-plane corrections are performed at the critical true latitude, θ_c. This seems simple in theory, but in practice, a numerical propagation takes finite time steps. Ultimately, a perfect periapsis, apoapsis, or θ_c crossing may not exist with the time step used. Instead, the controls must be implemented at the point nearest these ideal control angles. The true periapsis crossing is particularly difficult to find, since velocity

is faster near periapsis. Changes in anomaly are larger across a fixed time step near periapsis than near apoapsis, where the velocity is slower. Corrections may be performed near, but not exactly at, the optimal locations. This can result in the introduction of initial errors if corrections are not performed precisely at periapsis, apoapsis, or θ_c. This large difference in required ΔV between satellite one and the other satellites is likely due to the implementation errors in using a fixed time step. The control results for both satellite one and four will be presented and compared in order to investigate this further.

Table 3.7: Total ΔV magnitude over 28 days

Satellite	1	2	3	4
ΔV (m/s)	360.6	247.4	256.5	234.4

The errors in the orbital elements for satellite one are shown in Fig. 3.7. From Fig. 3.7a, it can be seen that on average, a, e, and i do not grow, but rather osculate around a mean value. However, in Fig. 3.7b, ω, Ω, and M grow between control cycles, but after each control period, the element errors are reduced to nearly zero. In other words, the control sequence corrects the actual orbit elements to match the desired orbit elements. As shown in Fig. 3.8, the red dashed line is the desired elements and the solid blue line is the actual elements. After each sequence of five control orbits, the actual elements converge on the desired element values. The initial jumps that occur at the beginning of each control phase for the in-plane elements (a, e, M, and ω) are caused by the application of the controls at a point close to, but not exactly at, periapsis. The errors that are introduced are eliminated in subsequent control orbits from the burns at apoapsis, where better accuracy is achieved due to the slower velocity near apoapsis.

In Fig. 3.8, the desired values for a, e, i, and ω are all constant, as described in Table 3.6. However, the RAAN (Ω) is drifting over time. The control phases capture the drift behavior and converge to the current RAAN value rather than the initial RAAN.

The errors in the orbital elements for satellite four are shown in Fig. 3.9. The errors follow the same trends as in Fig. 3.7 for satellite one. However, for satellite four, during the initial correction

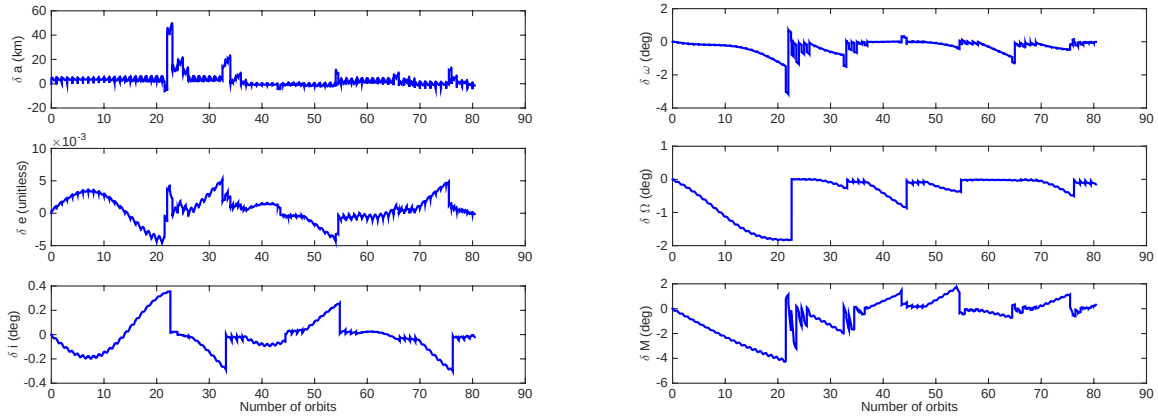

(a) Errors in a, e, and i

(b) Errors in ω, Ω, and M

Figure 3.7: Satellite one element errors for T_{r} controlling every four days

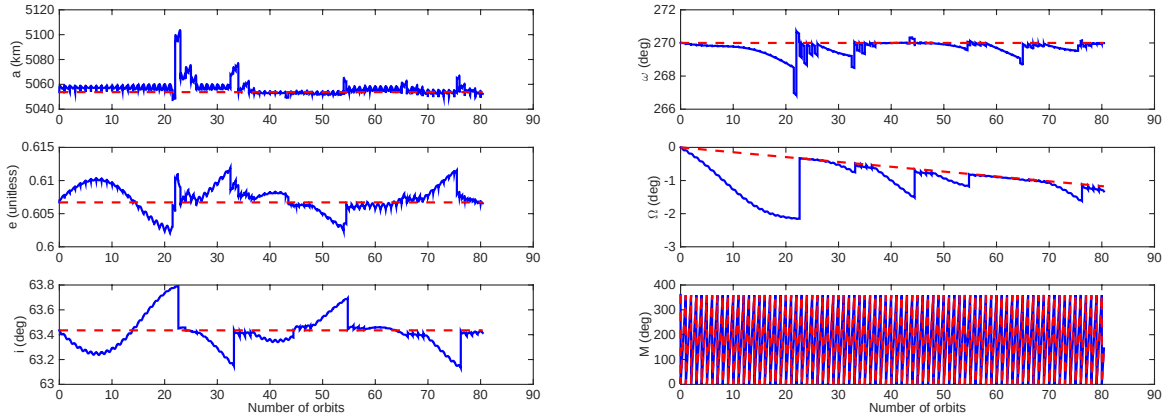

(a) Actual and desired a, e, and i

(b) Actual and desired ω, Ω, and M

Figure 3.8: Satellite one actual (solid) and desired (dashed) elements controlling every 4 days

orbit, the semi-major axis only jumps to an error of 10 km, compared to around 50 km for satellite one. Further investigation into the application of these control laws found that this error introduced into the semi-major axis from the impulsive orbit element corrections is dependent on how close the periapsis maneuver is performed relative to a true periapsis location of a true anomaly of 0°. The further off from periapsis, the larger the error introduced will be. The control laws are robust enough to absorb this error and correct the semi-major axis back to the desired value, but at the

cost of additional ΔV. Overshooting in the mean eccentricity (e), anomaly (M) and argument of periapsis (ω) align with the overshooting of the semi-major axis, especially considering those are all in-plane components that are affected by maneuvers at periapsis.

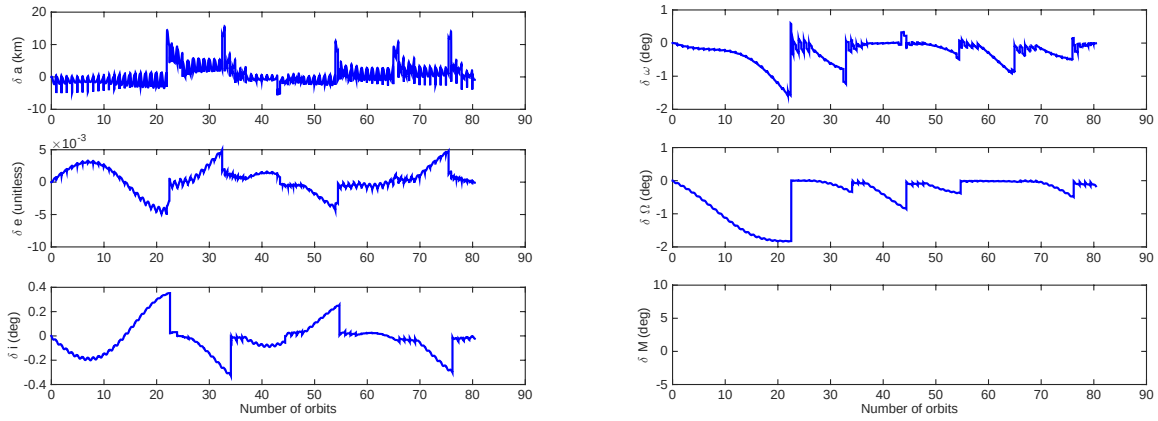

(a) Errors in a, e, and i

(b) Errors in ω, Ω, and M

Figure 3.9: Satellite four element errors for T_{r} controlling every four days

3.3.3.2 Constellation Lifetime Prediction

In order to predict the lifetime of a flower constellation at the Moon, two pieces of information are needed: the fuel required and the fuel available for each satellite. The fuel required per 27-day repetition period, per satellite was given in Table 3.7. The fuel required and available depends on many factors, but some assumptions can be made to estimate how long a flower constellation can be maintained at the Moon. Two primary factors that affect cubesat fuel consumption are overall mass and the type of engine or propellant used. Figure 3.10, from Reference 9 plots propellant mass required vs. ΔV for various types of propellant. This plot assumes a 4 kg cubesat. It can be seen that as the specific impulse (I_{sp}) increases, the mass of propellant required decreases.

In order to predict constellation lifetime, further assumptions must be made. One assumption is how much fuel the satellite will carry. The type of thruster used will also affect the lifetime. In order to provide a baseline constellation lifetime prediction, 1 kg of fuel is assumed, and the four

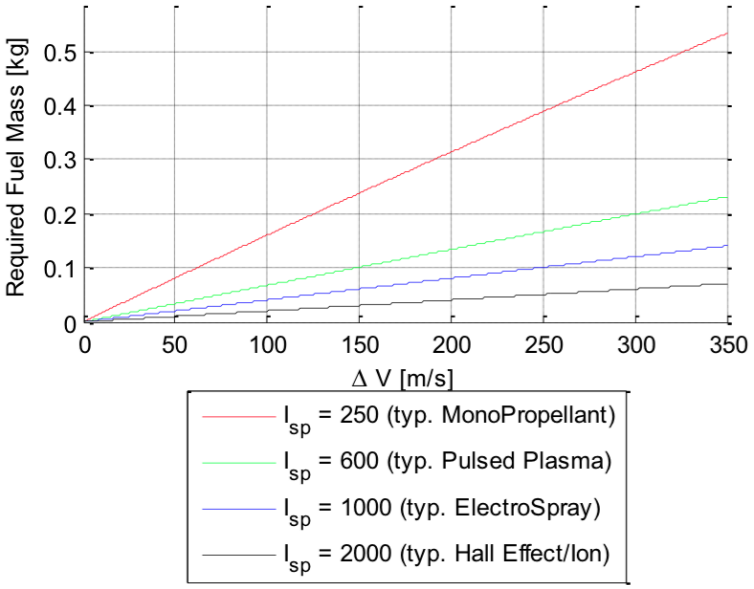

Figure 3.10: cubesat fuel use [9]

thruster types presented in Fig. 3.10 are investigated. The ΔV costs for each satellite for corrections every four days over a 28-day period are averaged across the four satellites and then fitted to a linear curve to predict fuel use over an extended period of time. Figure 3.10 also provides linear relationships between ΔV and propellant mass that can be used to find how much total ΔV that 1 kg of each type of propellant can produce. This allows for predictions for constellation lifetime based on 1 kg of fuel for monopropellant, pulsed plasma, electrospray, and Hall effect thrusters. This lifetime prediction is presented visually in Fig. 3.11

In Fig. 3.11, the red curve in the bottom left of the plot is the actual calculated average ΔVs after every four days for 28 days. The black curve is the linear curve fit produced from the first 28 days of calculated burns, extrapolated for 800 days. It can be seen in Fig. 3.11 that for a monopropellant thruster and 1 kg of fuel, the constellation can last nearly 100 days. As the thruster efficiency increases in the form of a higher I_{sp}, the constellation lifetime increases. A pulsed plasma thruster can support the constellation for just over 200 days, the electrostatic thruster extends the lifetime to around 370 days, and the Hall thruster provides the longest constellation lifetime at over 750 days.

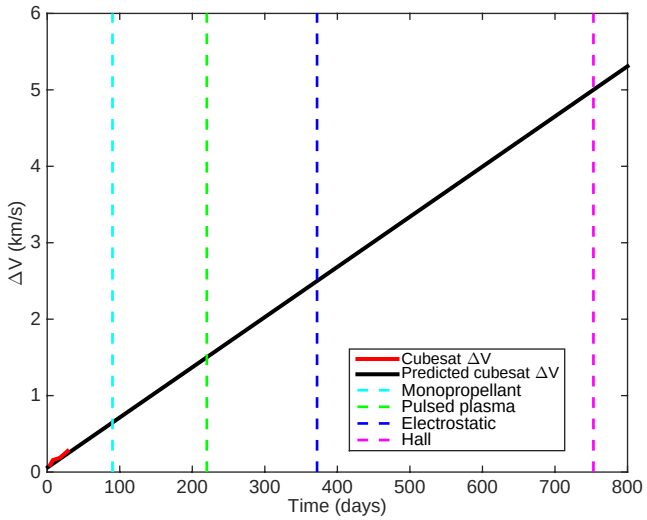

Figure 3.11: Single-petal FC lifetime prediction

Chapter 4

Multi-Petal Flower Constellations

In contrast to the previous section on single-petal flower constellations, a multi-petal constellation is studied in this section. There will now be multiple inertial orbits, and the more traditional RAAN phasing of Eq. (2.5) is used. Once again, in order to match the repeat ground tracks of Russell in Reference[12], a 73-1-4 constellation is studied, with a periapsis height of 250 km is used throughout this chapter.

4.1 Deployment Scheme

In the deployment of a multi-petal flower constellation, plane change maneuvers will be required. Unfortunately, plane change maneuvers are often very costly. Therefore, it is desired to find an optimal plane change maneuver for deploying a flower constellation of satellites at the Moon where the individual RAAN changes required could be as large as 90°, with a cumulative RAAN distribution of up to 360° for a symmetric constellation. The optimal maneuvers need only place the mothercraft in the desired orbit with the specified RAAN. Once in that orbit, the mothercraft can wait until it is at the proper mean anomaly to deploy the small satellite in order to achieve the phasing in both M and Ω defined by Eq. (2.4) and Eq. (2.5) or (2.6).

4.1.1 Baseline Cost

A one-impulse maneuver is the simplest plane change maneuver and is fairly robust to third body effects that would be prevalent at the Moon. A one-impulse maneuver will, therefore, serve

as the baseline cost for large plane change maneuvers at the Moon. Simple expressions for the ΔV required for a given $\Delta\Omega$ exist for circular orbits. However, flower constellation orbits are usually highly elliptical. The orbits are also inclined, so that a joint inclination and RAAN change is required. A one-impulse plane change must be performed at one of the two nodes where the initial and desired orbit planes intersect. This optimal point is found numerically after looping through various values of the mean anomaly in two neighboring flower constellation orbits. The point where the components of the position vectors are equal is one of the nodes. Two node possibilities will exist; the node located at the larger radius magnitude will be more optimal as the local velocity will be lower, thus resulting in a decreased plane change cost. Two neighboring orbits from a 73-1-4 flower constellation are shown in Fig. 4.1 with the two nodes for one-impulse maneuvers shown by the red dots. The cost of this one-burn plane change can be found by calculating the magnitude of the difference in the inertial velocity vectors between the two orbits at the node.

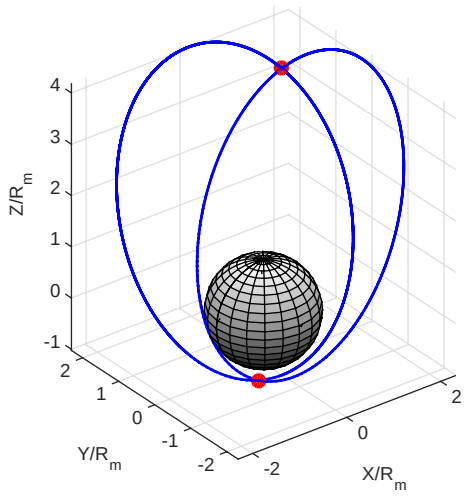

Figure 4.1: Nodes for one-impulse maneuvers

One-burn plane changes are the simplest maneuver to alter the plane of an orbit. It is known that three-impulse plane change maneuvers (i.e. bi-elliptic maneuvers) are usually optimal over one-impulse plane changes[17]. A bi-elliptic plane change is shown in Fig. 4.2, where the majority of the plane change occurs at the second maneuver, and a small amount occurs at the first and last

burns.

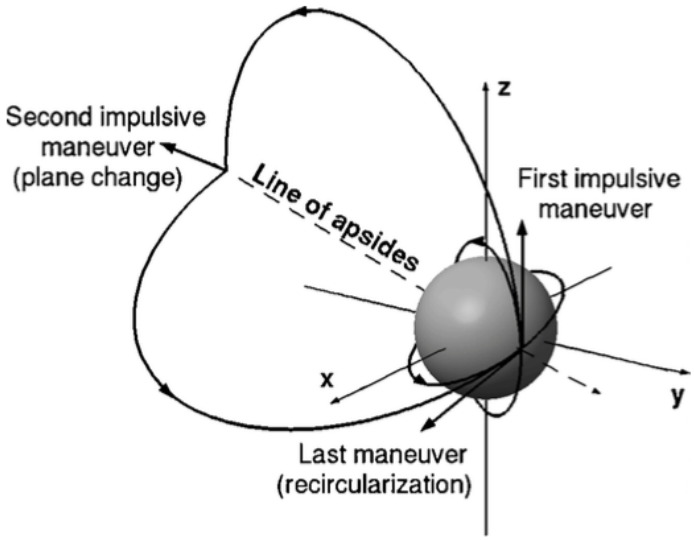

Figure 4.2: Bi-elliptic three-burn plane change[17]

4.1.2 Optimal Three-Burn Maneuver

While bi-elliptic plane change maneuvers are known to be optimal for large plane changes, the large transfer orbits of a bi-elliptic plane change maneuver can be problematic at the Moon, where third body effects from the Sun and Earth can cause large perturbations in the transfer orbits. In fact, only a simple one-impulse maneuver is really feasible at the Moon, unless the third body effects are used to the advantage of the maneuver[17]. In Reference 17, it has actually been shown that for plane change maneuvers larger than 60°, a third-body-driven transfer is optimal over the one-impulse burn. However, the trade-off for these fuel savings is a large increase in time to complete the maneuver. The maneuver is also dependent upon the location of the primary body relative to the secondary bodies during the maneuver. Therefore, the first RAAN change required for deployment would occur in a very different celestial geometry than the subsequent maneuvers. The increased time and complexity of performing third-body-driven transfers is not desirable for establishing a flower constellation at the Moon, unless it is the only viable option based on fuel requirements.

As a compromise between a true bi-elliptic plane change and a one-impulse maneuver, a modified bi-elliptic three-burn plane change with only a slight increase in the semi-major axis is proposed as a potentially optimal means of performing a large RAAN change between two orbits in the flower constellation. It is assumed that the mothercraft is initially in one of the desired flower constellation orbits, and has already deployed the first cubesat at the appropriate mean anomaly. The deployment of the remaining $N_s - 1$ satellites will be investigated through the use of transfer orbits in a small bi-elliptic method. The semi-major axis of the transfer orbit is restricted in order to avoid significant third-body effects during the transfer. The burn sequence begins with a burn in the first flower constellation orbit to raise the orbit, followed by a burn near apoapsis to perform the majority of the desired plane change, and finishing with a burn to match the desired flower constellation orbit in the second flower constellation plane. It is assumed that the mothercraft is performing all three burns in the bi-elliptic maneuver in order to save the fuel in the small satellites for constellation maintenance maneuvers.

The optimal three-burn maneuver sequence is established as an optimization problem to be solved using MATLAB's built-in constrained optimizer, `fmincon.m`. The goal of this optimization problem is to find the optimal values of the following parameters:

- M_1: Mean anomaly in initial FC orbit at which to perform first impulsive burn
- $\Delta \boldsymbol{V}_1$: Inertial delta-V vector for first impulsive burn
- M_T: Mean anomaly in transfer orbit at which to perform second impulsive burn
- $\Delta \boldsymbol{V}_2$: Inertial delta-V vector for second impulsive burn
- M_2: Mean anomaly in final FC orbit at which to perform third impulsive burn
- $\Delta \boldsymbol{V}_3$: Inertial delta-V vector for third impulsive burn

Intuitively, it is expected that M_1 will be near periapsis and that the first burn, $\Delta \boldsymbol{V}_1$, will raise the apoapsis of the orbit. Some of the plane change will be accomplished by $\Delta \boldsymbol{V}_1$ and $\Delta \boldsymbol{V}_3$,

but both of these maneuvers will primarily be responsible for adjusting the size (semi-major axis) and shape (eccentricity) of the orbits. The majority of the plane change will occur with $\Delta \boldsymbol{V}_2$, with this burn doing very little to change either the size or shape of the transfer orbit. The third burn, $\Delta \boldsymbol{V}_3$ is also expected to occur near periapsis as this maneuver will lower the orbit back to the flower constellation semi-major axis and eccentricity values.

Scaling is very critical in optimization. All parameters to be optimized–as well as bounds and constraints on the system–must all be the same order of magnitude. For this problem, all values are desired to be between ± 1. In order to achieve this scaling, normalization is used for parameters that would otherwise fall outside of the ± 1 scale limits. The mean anomaly is normalized by 2π with a lower bound of 0 and an upper bound of 1. The $\Delta \boldsymbol{V}$ components do not require normalizing as they are already bounded to be between ± 0.5 km/s.

The cost function for this problem is simply the total ΔV required for the three-burn maneuver. As such, the cost is given by the sum of the magnitudes of the individual burns. The first and second burn ΔV components are parameters to be optimized. The third burn ΔV_3 is simply determined by the magnitude of the difference between the velocity vector at M_2 in the final flower constellation orbit and the velocity vector at the end of the second transfer orbit. The cost function is given by Eq. (4.1).

$$f = \Delta V_1 + \Delta V_2 + \Delta V_3 \tag{4.1}$$

There are also some constraints on this problem in addition to the bounds that were placed on the optimization parameters. These constraints take the form of either equality constraints or inequality constraints. The equality constraints state that the components of the inertial position vectors at the end of the second transfer orbit must match the components of the position vector at M_2 in the final flower constellation orbit. The position vectors are normalized by the semi-major axis of the flower constellation orbits for scaling purposes, as given by Eq. (4.2)

$$\boldsymbol{g} = \frac{\boldsymbol{R}_{\mathrm{T2_f}}}{a_{\mathrm{FC}}} - \frac{\boldsymbol{R}_{\mathrm{FC2_{M_2}}}}{a_{\mathrm{FC}}} = \boldsymbol{0} \tag{4.2}$$

There are several inequality constraints on the problem. The first constraint is that the

eccentricities of the transfer orbits must be less than one to ensure an elliptic transfer orbit. The second constraint is that the radius of periapsis of the transfer orbits must be larger than the radius of the Moon in order to ensure that the transfer orbits do not intersect the lunar surface. This constraint uses the radius of the Moon to normalize for proper scaling. The final inequality constraint is that the semi-major axis of the transfer orbits must be less than a specified semi-major axis limit. This constraint is normalized by the semi-major axis of the individual transfer orbits to ensure proper scaling. The inequality constraints are summarized by Eq. (4.3)

$$h_1 = e_{\mathrm{T1}} - 1 \leq 0 \tag{4.3a}$$

$$h_2 = e_{\mathrm{T2}} - 1 \leq 0 \tag{4.3b}$$

$$h_3 = \frac{R_{\mathrm{m}} - r_{\mathrm{p,T1}}}{R_{\mathrm{m}}} \leq 0 \tag{4.3c}$$

$$h_4 = \frac{R_{\mathrm{m}} - r_{\mathrm{p,T2}}}{R_{\mathrm{m}}} \leq 0 \tag{4.3d}$$

$$h_5 = \frac{a_{\mathrm{T1}} - a_{\max}}{a_{\mathrm{T1}}} \leq 0 \tag{4.3e}$$

$$h_6 = \frac{a_{\mathrm{T2}} - a_{\max}}{a_{\mathrm{T2}}} \leq 0 \tag{4.3f}$$

Within the confines of the small bi-elliptic strategy employed in this study, there exist trade-offs between the fuel spent in the first burn to raise apoapsis and fuel savings in changing the RAAN at a larger radius of apoapsis where the velocity is smaller. However, the larger the semi-major axis of the transfer orbit, the larger both ΔV_1 and ΔV_3 will become. Additionally, large orbits about the Moon are greatly impacted by third-body perturbations from the Sun and Earth. The limit given to the semi-major axis of the transfer orbits, $a_{\max}$, will greatly impact the solution. The larger $a_{\max}$ is, the lower the overall cost, since the largest burn, ΔV_3 will decrease. However, it is desired for the transfer orbits to remain relatively small in order to avoid significant third-body perturbations. Perturbations are not included in this optimization, with the assumption that small errors that would accumulate over the transfer duration can be corrected for either by the mothercraft once in the final orbit, or by the children craft after deployment in the orbit maintenance maneuvers.

4.2 Numerical Simulation

The simulation of a multi-petal flower constellation is broken into three mission portions: deployment, mothercraft maneuver, and longterm orbit maintenance. The simulations of this chapter, as well as Section 3.3 utilize original MATLAB code as well as the publicly available `lprop.m` MATLAB script for predicting the evolution of lunar orbits, written by David Eagle. The code utilizes the LP150q 50 × 50 lunar gravity model, as well as point mass influences from the Earth and Moon.

4.2.1 Deployment

The initial flower constellation to be studied is a 73-1-4 constellation with a height of periapsis of 250 km. The orbital elements for the satellites in this constellation are summarized in Table 4.1.

Table 4.1: Orbital elements for 73-1-4 multi-petal flower constellation satellites

Satellite	a (km)	e	i (deg)	ω (deg)	Ω (deg)	M_0 (deg)
1	5053.73	0.60670	63.4	270	0	0
2	5053.72	0.60670	63.4	270	270	180
3	5053.72	0.60670	63.4	270	180	0
4	5053.72	0.60670	63.4	270	90	180

The baseline cost of a one-burn RAAN change is calculated and found to be 0.93084 km/s. For a small bi-elliptic method to be optimal over the one burn strategy, it must have a total cost less than 0.93084 km/s. Initially, the limit on the transfer orbit semi-major axis is set to 9000 km. The total cost for this maneuver is found to be 0.686234 km/s and is, therefore, optimal over the one-burn maneuver with a cost savings of 0.24460 km/s. The final values for the optimization parameters are summarized in Table 4.2.

The trajectories for this optimal three-burn maneuver are shown in Fig. 4.3, with the first flower constellation orbit shown in blue. The mothercraft remains in this orbit until it reaches M_1, at which point the first burn is implemented; this point is marked by the blue asterisk. After the

Table 4.2: Final values of optimization parameters for $a_{\max} = 9000$ km

M_1 (deg)	ΔV_{1_x} (km/s)	ΔV_{1_y} (km/s)	ΔV_{1_z} (km/s)	M_T (deg)	ΔV_{2_x} (km/s)	ΔV_{2_y} (km/s)	ΔV_{2_z} (km/s)	M_2 (deg)
338.32	0.047816	-0.055690	-0.117178	154.28	0.171642	0.182678	-0.277158	40.97

first burn, the mothercraft is on the first transfer orbit, shown in green. The mothercraft remains on this orbit until M_T is reached, at which point the second burn is performed and indicated by the green asterisk. After the second burn, the mothercraft is on the second transfer orbit, shown in cyan. The mothercraft remains in this orbit until is reaches a position corresponding to M_2 in the final flower constellation orbit, shown in red. This point is marked by the red asterisk and is the location of the third burn. The third burn matches the mothercraft velocity to the desired velocity at M_2 in the final flower constellation orbit. While not a constraint on the problem, the first and second transfer orbits have nearly matching orbital elements with the exception of RAAN and inclination, as these were desired to be changed in the maneuver. The orbital elements of the transfer orbits are summarized in Table 4.3.

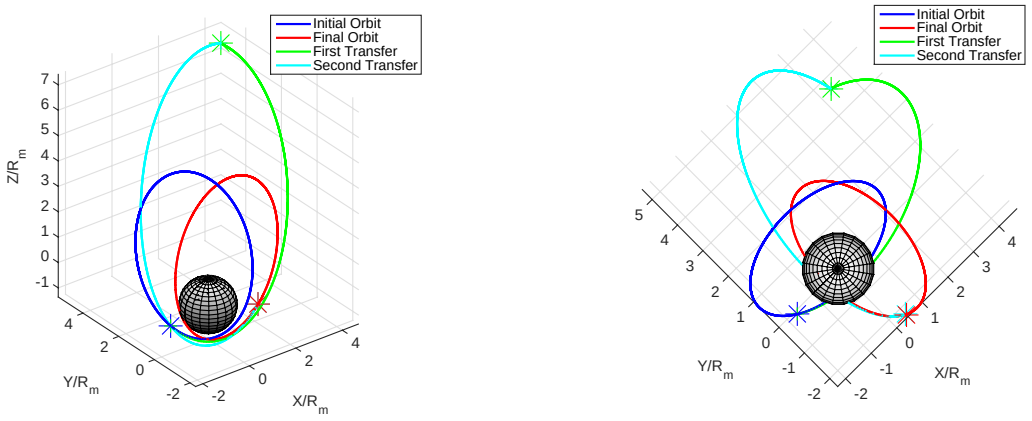

(a) Isometric view

(b) Polar view

Figure 4.3: Optimal three-burn orbits for $a_{\max} = 9000$ km

Ultimately, the limit placed on the semi-major axis of the transfer orbits significantly alters the optimal solution that can be found. The larger the semi-major axis of the transfer orbit,

Table 4.3: Orbital elements for transfer orbits for $a_{\max} = 9000$ km

Transfer Orbit	a (km)	e	i (deg)	ω (deg)	Ω (deg)	M_0 (deg)
1	8985.24	0.75436	63.50	253.38	0.01	352.45
2	8994.71	0.72790	65.16	293.49	270.89	182.38

the less costly the maneuver. However, the larger transfer orbits are subjected more to third-body perturbations and these maneuvers may result in larger initial corrections by the flower constellation satellites after deployment. It is desired to determine the semi-major axis limit at which the one-burn maneuver becomes more optimal over the three-burn transfer orbit. As the semi-major axis limit becomes smaller, the bi-elliptic nature of the transfer orbits no longer holds since the transfer orbit is not allowed to be much larger than the flower constellation orbits themselves. This change occurs approximately at a semi-major axis limit of 5200 km. However, even in these schemes, a three-burn maneuver is still shown to be optimal over a one-burn maneuver. Again, the baseline cost is 0.93084 km/s. When the limit on the transfer orbits semi-major axis is set to 5200 km the total cost for the three-burn maneuver is found to be 0.86228 km/s and is, therefore, optimal over the one-burn maneuver with a cost savings of 0.06855 km/s. The final values for the optimization parameters are summarized in Table 4.4.

Table 4.4: Final values of optimization parameters for $a_{max} = 5200$ km

M_1 (deg)	ΔV_{1_x} (km/s)	ΔV_{1_y} (km/s)	ΔV_{1_z} (km/s)	M_T (deg)	ΔV_{2_x} (km/s)	ΔV_{2_y} (km/s)	ΔV_{2_z} (km/s)	M_2 (deg)
158.32	0.067519	.152548	-0.376945	141.34	0.178413	0.088650	-0.398746	25.34

While still optimal over the one burn maneuver, the stricter semi-major axis limit causes the transfer orbits to take on a different form, as shown in Fig. 4.4. With a small semi-major axis limit, the second transfer orbit is nearly the same as the second flower constellation orbit, but with a small semi-major axis difference.

The orbital elements of the two transfer orbit elements are summarized in Table 4.5. It can be observed in Fig. 4.4 and Table 4.4 that the first burn, shown by the blue asterisk, is performed

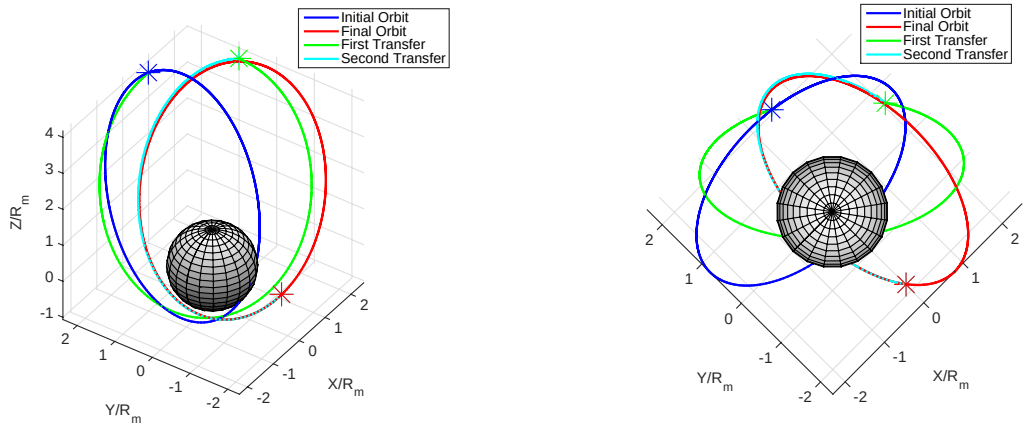

(a) Isometric view

(b) Polar view

Figure 4.4: Optimal three-burn orbits for $a_{\max} = 5100$ km

near apoapsis of the first orbit, instead of closer to periapsis in Fig. 4.3. The periapsis of the first transfer orbit is only slightly raised by the first burn to a semi-major axis of 5198.66 km. Almost a full orbit is completed in the first transfer orbit before the second maneuver is made. This second burn occurs near apoapsis of the final flower constellation orbit, as shown by the green asterisk. After the second burn, the orbit elements of the second transfer orbit almost match the desired elements for the final flower constellation orbit. The second transfer orbit, plotted in cyan, is nearly on top of the final flower constellation orbit shown in red. The third burn, marked by the red asterisk, simply matches the mothercraft to the orbital elements of the flower constellation orbit.

The previous simulations have assumed a 73-1-4 constellation, so that there are four orbit planes, each at a 90° RAAN separation. However, as N_s is increased, the $\Delta\Omega$ between orbits decreases. It is desired to know if the three-burn method is always optimal over the one-burn method. For a semi-major axis limits of 9000 and 5200 km, the parameter N_s is varied from four to twenty and the cost of the three-burn maneuver is compared to a one-burn maneuver. The results are plotted in Fig. 4.5. The values or $\Delta\Omega$ that correspond to the values of N_s are also plotted.

It can be seen in Fig. 4.5a, that the initial difference between the one-burn and three-burn

Table 4.5: Orbital elements for transfer orbits for $a_{\max} = 5200$ km

Transfer Orbit	a (km)	e	i (deg)	ω (deg)	Ω (deg)	M_0 (deg)
1	5198.66	0.60928	65.27	268.93	317.96	222.03
2	5101.79	0.60818	63.43	270.67	269.99	205.59

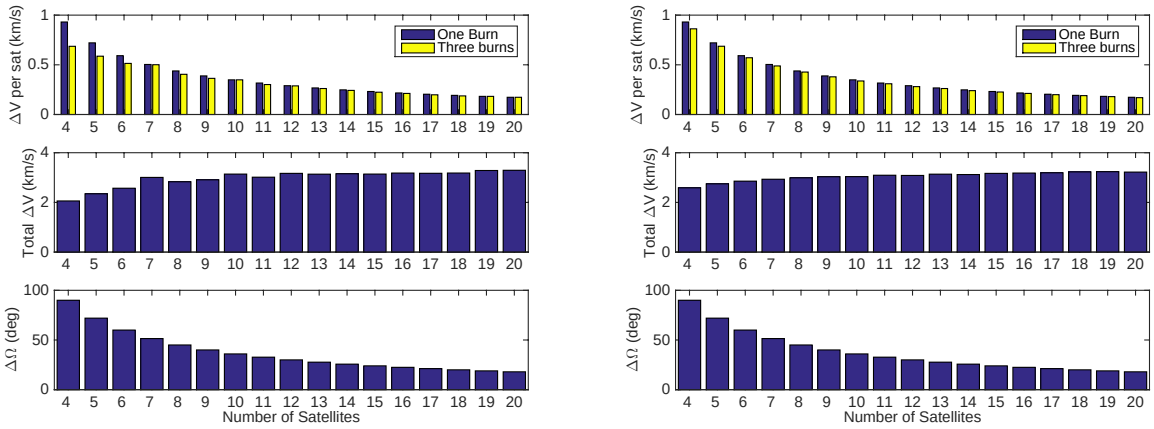

(a) $a_{max} = 9000$ km

(b) $a_{max} = 5200$ km

Figure 4.5: Maneuver costs for various values of N_s

maneuver for $a_{\max} = 9000$ km is greater than in Fig. 4.5b for $a_{\max} = 5200$ km. Regardless of the semi-major axis limit, as the number of satellites is increased, the RAAN change required per satellite decreases and the cost of the three-burn maneuver approaches the cost of the one-burn maneuver. However, the three-burn maneuver always less than or equal to the one-burn method.

It was also desired to observe trends in the cost for the establishment of the entire constellation as the number of satellites varied. For the semi-major axis limit of 9000 km, the general trend is that the total cost grows as the number of satellites increases, due to the increased number of maneuvers. However, there are some interesting fluctuations in the total cost for eight, nine, and eleven satellites. It is actually less expensive to establish an eight or nine satellite constellation than one with only seven satellites. Likewise, it costs less to create an eleven satellite constellation compared to a ten satellite constellation. For the semi-major axis limit of 5200 km, the general trend of increasing total cost is more consistent than for the semi-major axis limit of 9000 km.

The only deviants from the trend are a ten satellite constellation, which is equal in cost to a nine satellite constellation, as well as a twelve satellite constellation, which is equal in cost to an eleven satellite constellation.

Ultimately, for any number of satellites, N_s, a three-burn maneuver should be used to deploy the individual satellites in the constellation. The larger the semi-major axis limit, the less costly the three-burn maneuver. However, the larger the transfer orbits, the more prominent the third-body perturbations will be, perhaps requiring larger initial corrections by the flower constellation satellites after deployment. As is true in all optimization problems, the optimal solution is dependent upon the requirements of the problem at hand.

4.2.2 Mothercraft Orbit Maneuver

Once the flower constellation has been fully deployed, the mothercraft must maneuver to a long-term communications orbit. The requirement of this orbit are that the mothercraft must periodically pass by all of the children craft in order to communicate with them and then relay that information back to the Earth. The flower constellation satellites have limited communications range capability, necessitating the mothercraft to act as a relay point. A polar orbit for the mothercraft has been selected as it maintains the same symmetry as the flower constellation about the spin axis of the Moon. The semi-major axis is desired to be larger than the flower constellation orbit semi-major axis so that there is a period difference. This period difference will allow the mothercraft to travel by all children satellites rather than maintaining the same relative positions to the children satellites were the semi-major axis to match. The long-term mothercraft orbit will also have an argument of periapsis of 270° and a RAAN equal to that of the final child satellite that it deployed. The RAAN will drift with time due to lunar perturbations and this motion will not be controlled against, so that the initial RAAN is not a critical parameter. Therefore, to minimize fuel costs in this maneuver, the RAAN will not be changed from the final flower constellation orbit to the long-term mothercraft orbit.

Once again, a 73-1-4 flower constellation is studied. The desired semi-major axis for the

long-term mothercraft orbit is chosen to be 10% larger than the flower constellation semi-major axis. As it will be shown later, it is the inclination change from the critical inclination of 63.4° to a polar inclination of 90° that drives the cost of this maneuver. Therefore, the semi-major axis difference used is almost arbitrary.

The initial mothercraft orbit elements are the same as the final flower constellation orbit. The desired elements are the same except for at a polar inclination with a 10% larger semi-major axis. The initial and final elements for the mothercraft are summarized in Table 4.6.

Table 4.6: Initial and final mothercraft orbits

Orbit	a (km)	e	i (deg)	ω (deg)	Ω (deg)
Initial Orbit	5053.72	0.60670	63.4	270	90
Final Orbit	5559.10	0.60670	90	270	90

The simplest way to move the mothercraft into the desired orbit is to first perform one orbit with small burns in the along-track ($\hat{o}_\theta$) direction at both periapsis and apoapsis to raise the semi-major axis of the orbit. The costs of these burns are found using the impulsive orbit element control equations Eq. (3.13a) and Eq. (3.13b) with Δe set to zero. Once the desired semi-major axis is obtained, the plane change maneuver can be performed. It is desired to perform this maneuver second as the velocity will be smaller in the larger orbit, decreasing the cost of the maneuver. The location at which to perform the plane change maneuver will be governed by Eq. (3.10a) for the critical angle, θ_c at which plane change maneuvers are optimal. In this scenario, the RAAN change, $\Delta\Omega$ is zero, so that θ_c is either 90° or 270°. This burn will occur in the out of plane ($\hat{o}_h$) direction and is computed using Eq. (3.10b). The total baseline cost for this sequence of maneuvers was found to be 0.61438 km/s.

Similarly to the deployment scheme discussed in Section 4.1, this maneuver also involves a costly large plane change. Therefore, it is likely that there is a three-burn transfer orbit maneuver to change both the inclination and semi-major axis that would be optimal over the series of impulsive burns just discussed. The same optimization strategy can be employed for this maneuver. The cost

functions and constraints remain unchanged from Eqs. (4.1), (4.2), and (4.3). The only difference between these two optimization problems is the initial and final orbits desired. It should also be noted that the impulsive burns for the baseline cost are all in the LVLH frame (as shown in Fig. 3.2) whereas the burns to be optimized in the three burn transfer orbit scheme are inertial velocities. However, when comparing magnitudes, the frames used are irrelevant.

The baseline cost for this maneuver was found to be 0.61438 km/s. For the three-burn transfer orbit method to be optimal over the impulsive burn series strategy, it must have a total cost less than 0.61438 km/s. The limit on the transfer orbits semi-major axis is set to 9000 km. The total cost for this maneuver is found to be 0.44432 km/s and is, therefore, optimal over the impulsive burn series with a cost savings of 0.17007 km/s. The final values for the optimization parameters are summarized in Table 4.7.

Table 4.7: Final values of optimization parameters for final mothercraft maneuver

M_1	ΔV_{1_x}	ΔV_{1_y}	ΔV_{1_z}	M_T	ΔV_{2_x}	ΔV_{2_y}	ΔV_{2_z}	M_2
(deg)	(km/s)	(km/s)	(km/s)	(deg)	(km/s)	(km/s)	(km/s)	(deg)
60.09	0.188626	0.019958	0.104139	301.89	-0.222992	-0.020811	-0.042360	25.02

The optimal trajectories for the three-burn transfer orbit maneuver are shown in Fig. 4.6. The initial mothercraft orbit is shown in blue. The mothercraft remains in this orbit until it reaches M_1, at which point the first burn is implemented. This point is marked by the blue asterisk. After the first burn, the mothercraft is on the first transfer orbit, shown in green. The mothercraft remains on this orbit until M_T is reached, at which point the second burn is performed. This point is marked by the green asterisk. After the second burn, the mothercraft is on the second transfer orbit, shown in cyan. The mothercraft remains in this orbit until is reaches a position corresponding to M_2 in the final mothercraft orbit, shown in red. This point is marked by the red asterisk and is the location of the third burn. The third burn matches the mothercraft velocity to the desired velocity at M_2 in the flower constellation orbit.

The orbital elements of the transfer orbits are summarized in Table 4.8. The cyan orbit in

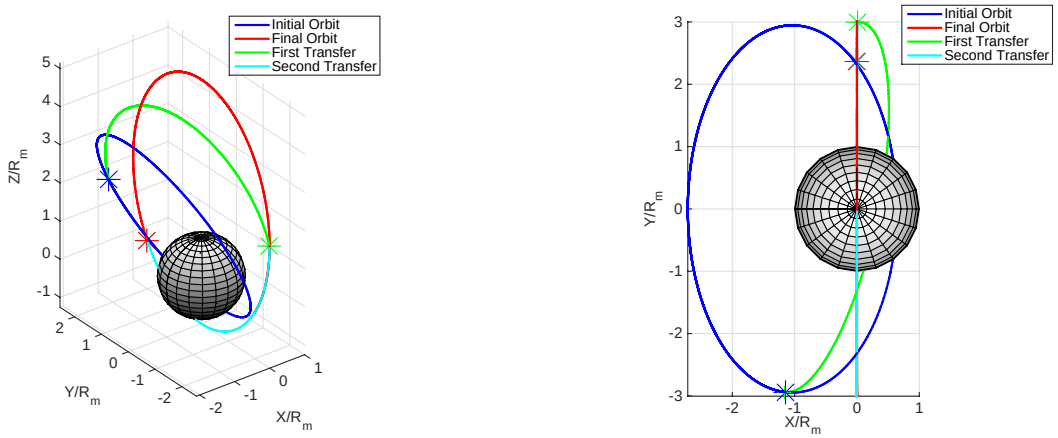

(a) Isometric view

(b) Polar view

Figure 4.6: Optimal three-burn orbits for $a_{\max} = 9000$ km

Fig. 4.6 shows that the second transfer orbit nearly matches the desired orbit. This is verified by comparing the orbital elements in Table 4.6 for the desired orbit to the elements in Table 4.8 for transfer orbit two. The final burn is a small burn that simply matches the two orbits more precisely.

Many orbits are feasible for the mothercraft long-term communications orbit, as long as the mothercraft periodically comes into communications range of all satellites in the constellation. The one example presented in this section is a good candidate orbit. The three-burn transfer orbit strategy used for this orbit can also be applied to other mothercraft maneuvers that may require large plane changes. Another approach for establishing a communications relay satellite would be to place an additional satellite (not the mothercraft) at one of the Earth-Moon stable Lagrangian points. The L1 Lagrangian point is between the Earth and the Moon and would, therefore, always have line-of-sight ability with both the Moon and Earth. The L2 Lagrangian point is behind the Moon, but a large enough orbit would form a sort of halo behind the Moon that would also always have line-of-sight ability with both bodies. A communications relay satellite at either Lagrangian point would require extended communications capability for the flower constellation satellites since the range between the Moon and L1 or L2 is significantly larger than the range between the

Table 4.8: Orbital elements for transfer orbits for $a_{\max} = 9000$ km

Transfer Orbit	a (km)	e	i (deg)	ω (deg)	Ω (deg)	M_0 (deg)
1	5390.58	0.60714	76.04	271.01	100.87	53.66
2	5559.42	0.60663	90.00	270.00	89.94	304.78

mothercraft and flower constellation satellites all in orbit at the Moon. Ultimately, this design choice would be specific to the mission requirements and the satellite capabilities.

4.2.3 Long-Term Orbit Maintenance

Just as in Section 3.3.3, now that the constellation has been deployed, the satellites will be subject to the various perturbations at the Moon. The impulsive orbit element controls presented in Section 3.2 are once again used to correct orbital elements to their desired values. The errors in the orbital elements are again found by subtracting the actual element values from the desired element values as given in Table 3.6.

The semi-major axis, eccentricity, and inclination are desired to remain constant. The argument of periapsis should also be constant as the frozen inclination eliminates the drift due to J_2, $\dot{\omega}$ given by Eq. (1.1b). However, the RAAN and mean anomaly will change with J_2, and as this is desired in a flower constellation, these drifts will not be controlled against. The drift in RAAN, $\dot{\Omega}$, is given by Eq. (1.1a) and the drift in initial mean anomaly, $\dot{M}_0$, is given by Eq. (1.1c). The term Δt is simply the elapsed time since the initial time, t_0, and n_{d} is the desired mean motion, calculated using the desired semi-major axis, a_{d}. The values for the initial orbit elements can be found in Table 4.1.

As in Section 3.3.3, in order to conserve fuel, the accuracy of the flower constellation orbits is sacrificed to a certain extent. The orbits will be corrected every four days over approximately one 27-day (one lunar day) repetition period for the constellation. Recall that the repetition period is the value T_{r} as given by Eq. (1.6) with N_{d} set to one lunar day. Each control sequence consists of five orbits.

4.2.3.1 Control Simulation Results

The relative orbits for the repetition period are shown in Fig. 4.7. The overall vase shape is maintained, although the perfect latticework of the relative orbits is compromised by the lunar perturbations and the drift that occurs between control periods. The difference between the flower constellation with full perturbations and only J_2 can be seen by comparing Fig. 4.7a with Fig. 2.5b. However, the lunar surface coverage of the constellation is still achieved, just without the exact repeat ground track nature that would occur with only J_2, or if controls were to be applied every orbit to constantly eliminate drift.

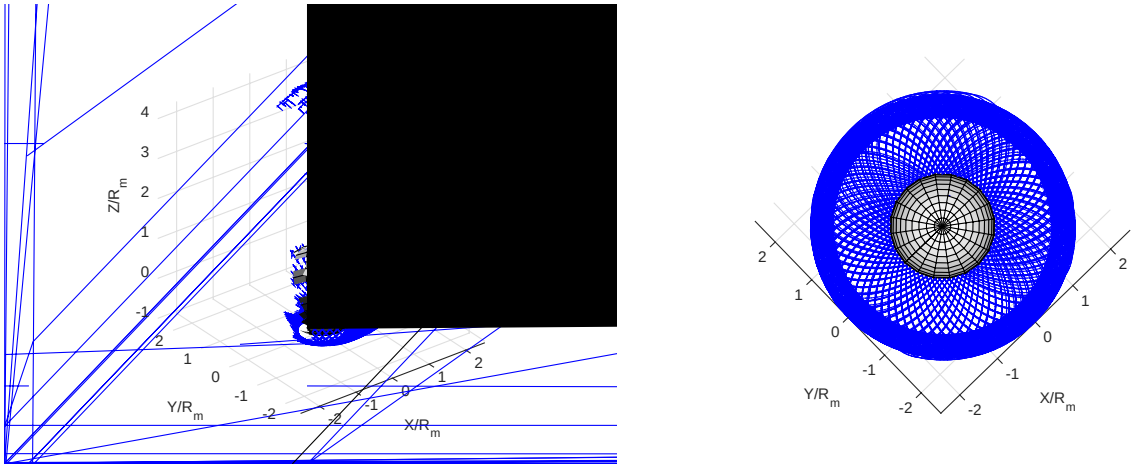

(a) Isometric view

(b) Polar view

Figure 4.7: 73-1-4 multi-petal FC relative orbits

The inertial orbits over the repetition period are shown in Fig. 4.8. It can be seen that the perturbations cause precession in the inertial orbits over the 27-day repetition period, by comparing Fig. 4.7a to Fig. 2.6b where only J_2 was included. Just as was the case with the single-petal constellation, the total control costs are sensitive to how close the corrections are applied relative to the desired locations of periapsis, apoapsis, and θ_c. Again, it was found that satellite one experienced the largest ΔV and after further investigation, it was found to be due, once again, to how close the in-plane corrections were performed relative to the actual periapsis crossing. This is an implementation challenge and is manifested in the higher control ΔV cost for satellite one

compared to the remaining satellites, as shown in Table 4.9. Since satellite one is the worst case, only the results of the control simulation for satellite one ($\Omega = 0°$) are presented in detail.

Table 4.9: Total ΔV magnitude over five control orbits

Satellite	1	2	3	4
ΔV (m/s)	360.6	219.3	201.5	231.8

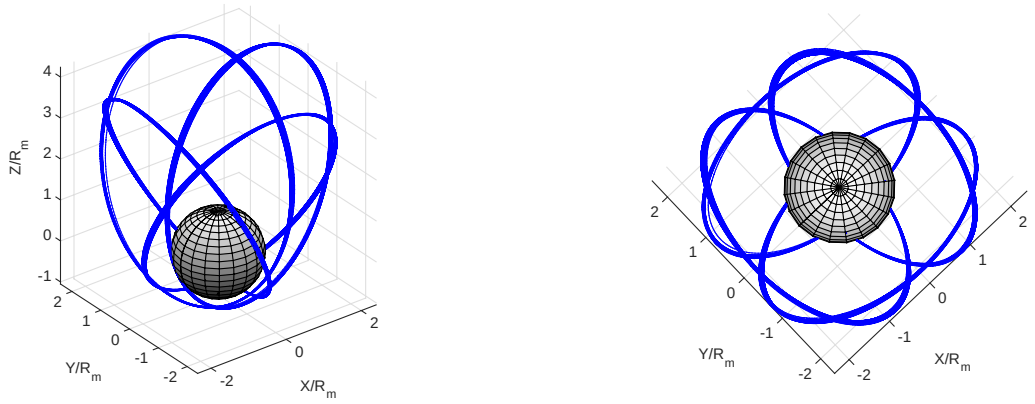

(a) Isometric view

(b) Polar view

Figure 4.8: 73-1-4 multi-petal FC inertial orbits

The errors in the orbital elements for satellite one are shown in Fig. 4.9. From Fig. 4.9a, it can be seen that on average, a, e, and i do not grow, but rather osculate around a mean value. However, in Fig. 4.9b, ω, Ω, and M grow over the first five days before the first control cycle is implemented. However, after each control period, the element errors are reduced to nearly zero. In other words, the control sequence corrects the actual orbit elements to match the desired orbit elements. This behavior is shown in Fig. 4.10. The red dashed line is the desired elements and the solid blue line is the actual elements. After each sequence of five control orbits, the actual elements converge on the desired element values. The initial jumps that occur at the beginning of each control phase for the in-plane elements (a, e, and ω) are all due to the application of the controls at a point near periapsis, but not exactly at periapsis. These errors that are introduced

are eliminated in subsequent control orbits from the burns at apoapsis, where better accuracy is achieved due to the slower orbital velocity near apoapsis.

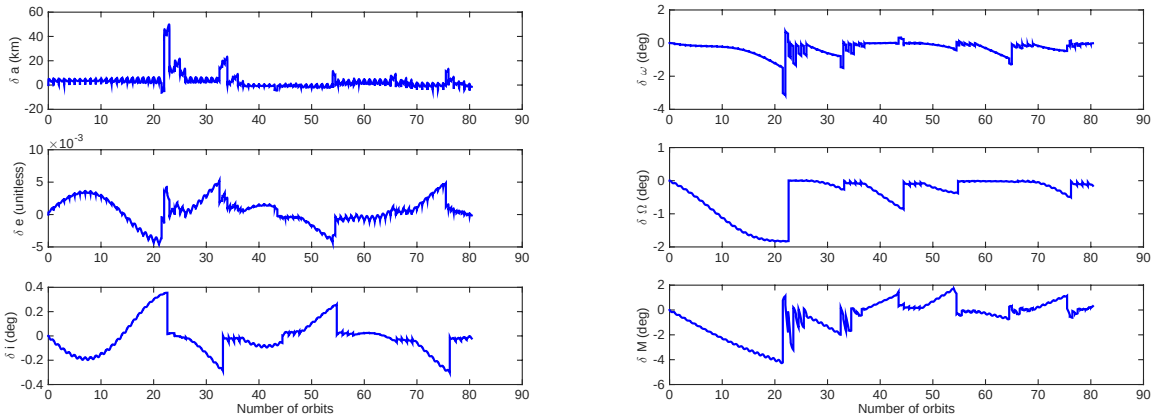

(a) Errors in a, e, and i

(b) Errors in ω, Ω, and ν

Figure 4.9: Satellite one element errors for T_{r} controlling every four days

In Fig. 4.10a, the desired values for a, e, i, and ω are all constant, as described in Table 3.6. However, the RAAN (Ω) is drifting over time. The control phase captures the drift behavior and converges to the current RAAN value rather than the initial RAAN, as shown in Fig. 4.10b.

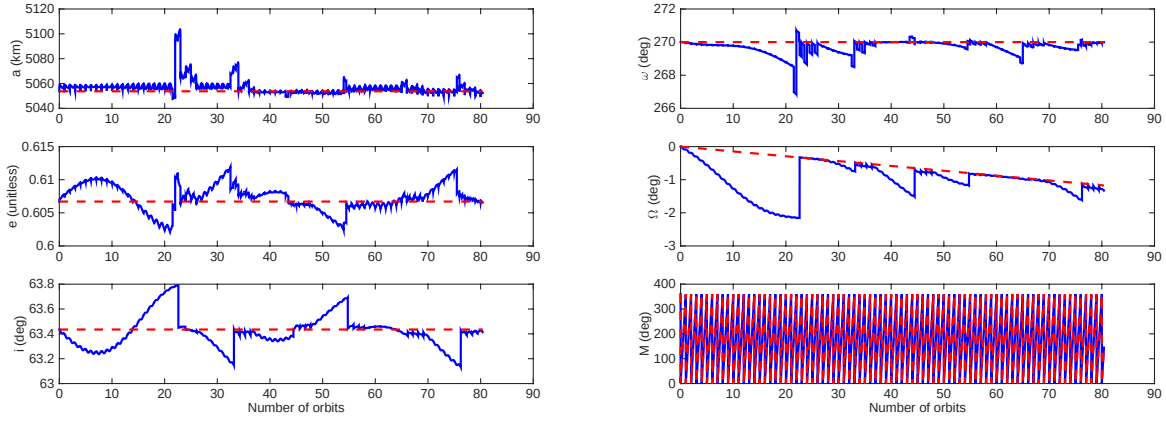

(a) Actual and desired a, e, and i

(b) Actual and desired ω, Ω, and ν

Figure 4.10: Satellite one actual (solid) and desired (dashed) elements controlling every four days

4.2.3.2 Constellation Lifetime Prediction

As was done in Section 3.3.3.2, the lifetime of the constellation is predicted. The fuel required per 27-day repetition period, per satellite was given in Table 4.9. The same assumptions made in Section 3.3.3.2 are used: the cubesat has a mass of 4 kg including 1 kg of fuel and uses either a monopropellant, pulsed plasma, electrospray, or hall effect thruster system. The same thruster parameters from Reference 9 given in Fig. 3.10 are used as well.

The ΔV costs for each satellite for corrections every four days over a 28-day period are averaged across the satellites and then fitted to a linear curve to predict fuel use over an extended period of time. The predictions for constellation lifetime based on 1 kg of fuel for monopropellant, pulsed plasma, electrospray, and hall effect thrusters are shown in Fig. 4.11

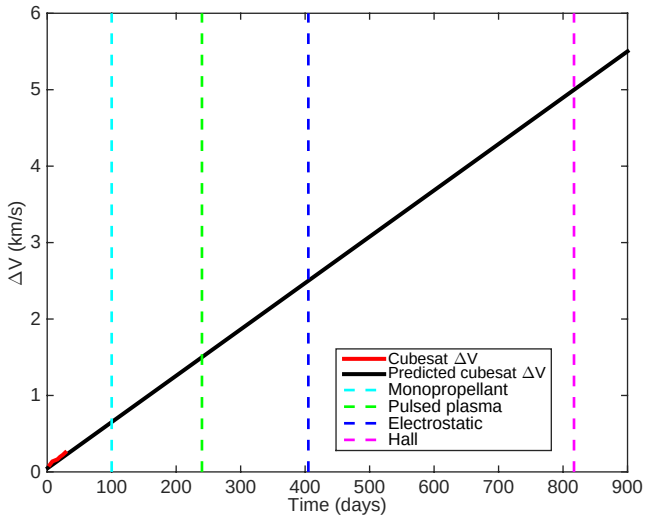

Figure 4.11: Single-petal FC lifetime prediction

In Fig. 4.11, the red curve in the bottom left of the plot is the actual calculated average ΔVs after every four days for 28 days. The black curve is the linear curve fit produced from the first 28 days of calculated burns, extrapolated for 900 days. By comparison to Fig. 3.11, it can be seen that the multi-petal constellation requires slightly less ΔV over time, extending the lifetime of the constellation. It can be seen in Fig. 4.11 that for a monopropellant thruster and 1 kg of fuel, the

constellation can last exactly 100 days. As the thruster efficiency increases in the form of a higher I_{sp}, the lifetime increases. A pulsed plasma thruster can support the constellation for 240 days, the electrostatic thruster extends the lifetime to just over 400 days, and the hall thruster provides the longest constellation lifetime at over 800 days.

Chapter 5

Conclusions

This work provided an initial investigation of the feasibility for establishing a flower constellation at the Moon. This constellation can take the form of either a single-petal constellation or a multi-petal constellation. Both constellations studied were 73-1-4 constellations with a height of periapsis of 250 km in order to provide a link with the repeat ground track orbits of Reference 12. The challenges of applying flower constellations to the Moon, optimal deployment schemes, and constellation lifetime and maintenance were all investigated.

Two significant differences for satellites about the Moon versus the Earth are the rotation periods and perturbations for the two bodies. The rotation period of the Earth is one sideral day, whereas, the rotation period of the Moon is 27.32 sidereal days. The rotation period of the central body directly affects the period of a flower constellation orbit. This resulted in very large orbits that were infeasible at the Moon for an $N_{\mathrm{d}} = 1$ constellation with a small number of petals. Instead, it was proposed that the number of petals be increased to a larger number ($N_{\mathrm{p}} > 50$), creating the new look of basket constellations when applied to the Moon. The perturbations at the Moon are significantly different than those at Earth. At Earth, the dominant perturbation is due to J_2. Since flower constellations are designed to be J_2 compatible, these constellations can be expected to have long lifetimes with low maintenance costs. However, the perturbations at the Moon are far more challenging. The dominant perturbation is not J_2, with higher order zonal and tesseral harmonics at near the same order of magnitude. Additionally, the Earth and Sun cause large third-body perturbations for orbits about the Moon. The additional lunar perturbations necessitate the need

for regular orbit maintenance maneuvers and will also limit the lifetime of the constellation.

In addition to the challenges faced once at the Moon, the deployment of a constellation at the Moon is also unique compared to deployment at Earth. At Earth, the constellation satellites can be launched individually, establishing the constellation over time. Launching several satellites to the Moon individually is too costly. Instead, the constellation satellites would likely be small satellites carried aboard a mothercraft. The mothercraft would then deploy the children craft into their appropriate orbit slots at the Moon. This requires a deployment strategy for establishing a constellation. For a single-petal constellation, the deployment is relatively simple and inexpensive as all satellites can be deployed into their string-of-pearls formation from a raised mothercraft orbit, using just the cubesat deployment mechanism to match the child craft to its desired orbit. Deploying a multi-petal constellation takes more creativity as multiple orbit planes are desired. A one-burn plane change maneuver can be performed by the mothercraft to move between sequential flower constellation orbits, but is known to not be optimal for larger plane change maneuvers. Alternatively, a three-burn transfer orbit sequence is investigated, with optimal solutions found using MATLAB's built-in constrained optimizer, `fmincon.m`. It was shown that a three-burn transfer orbit maneuver is always equal to or less costly than a one-burn maneuver for various RAAN separations as well as transfer orbit semi-major axis limits.

Once deployment of the constellation is complete, the mothercraft transitions into the role of communications relay between the constellation satellites and Earth. This is a simple maneuver for a single-petal constellation. The longterm mothercraft orbit is desired to match the flower constellation orbit with just an eccentricity offset. This is accomplished through a relatively inexpensive series of phase orbits. With the multi-petal constellation, the mothercraft is desired to move from the final flower constellation orbit to a polar orbit with a semi-major axis difference from the orbits in the flower constellation. Just as in the deployment of the multi-petal constellation, this maneuver requires a large and costly plane change. The same three-burn transfer orbit scheme is again shown to be an optimal solution to this maneuver.

After the constellation satellites and mothercraft are all in the correct orbits, the constella-

tion will be subject to the perturbations at the Moon and will require maintenance over time. An impulsive orbit element control law is used to correct the constellation orbit elements every five days for a 27 day repetition period. This simulation is run with both the single and multi-petal configurations. Once fuel costs are found in the form of required ΔVs, the lifetime of the constellation can be predicted. It was found that both constellations could be maintained for between around 100 and 800 days, depending on the efficiency of the thrusters used. This was for an assumed 4 kg cubesat with 1 kg of fuel. More fuel available would of course extend the lifetime of the constellation.

Overall, it has been demonstrated that flower constellations are indeed feasible at the Moon. In fact, the constellation can achieve a significant scientific mission with a lifetime of at least 90 days. While this investigation made many specific assumptions in the studies and simulations performed, the techniques can be generalized to any sort of constellation at any Moon or other celestial body. The perturbations and constellation configuration would differ based on the central body involved.

Bibliography

[1] Christopher Boshuizen, James Mason, Pete Klupar, and Shannon Spanhake. Results from the Planet Labs Flock Constellation. 2014.

[2] Dirk Brouwer. Solution of the problem of artificial satellite theory without drag. The Astronomical Journal, 64:378, 1959.

[3] Jean P. dos S. Carvalho, Rodolpho Vilhena de Moraes, and FB de A. Antonio. Non-sphericity of the moon and critical inclination. Earth, 3(10):6–102, 2009.

[4] David Folta and David Quinn. Lunar Frozen Orbits. American Institute of Aeronautics and Astronautics, August 2006.

[5] E. Gill, P. Sundaramoorthy, J. Bouwmeester, B. Zandbergen, and R. Reinhard. Formation flying within a constellation of nano-satellites: The QB50 mission. Acta Astronautica, 82(1):110–117, January 2013.

[6] M Hornyi, Z Sternovsky, M Lankton, C Dumont, S Gagnard, D Gathright, E Grn, D Hansen, D James, S Kempf, and others. The Lunar Dust Experiment (LDEX) Onboard the Lunar Atmosphere and Dust Environment Explorer (LADEE) Mission. Space Science Reviews, 185(1-4):93–113, 2014.

[7] W. Lan. Poly Picosatellite Orbital Deployer Mk III ICD. Preliminary 0, California Polytechnic State University, San Luis Obispo, CA, August 2007.

[8] RH Lyddane. Small eccentricities or inclinations in the Brouwer theory of the artificial satellite. The Astronomical Journal, 68:555, 1963.

[9] Anne Dorothy Marinan. From CubeSats to constellations: systems design and performance analysis. PhD thesis, Massachusetts Institute of Technology, 2013.

[10] Daniele Mortari. Flower Constellations as rigid objects in space. ACTA Futura, 2:7–22, 2006.

[11] Daniele Mortari, Matthew P. Wilkins, and Christian Bruccoleri. The Flower Constellations. 2004.

[12] Ryan P. Russell and Martin Lara. Long-Lifetime Lunar Repeat Ground Track Orbits. Journal of Guidance, Control, and Dynamics, 30(4):982–993, July 2007.

[13] Hanspeter Schaub. Analytical mechanics of space systems. AIAA education series. American Institute of Aeronautics and Astronautics, Reston, VA, 2nd ed edition, 2009.

[14] Hanspeter Schaub and Kyle T. Alfriend. Impulsive Feedback Control to Establish Specific Mean Orbit Elements of Spacecraft Formations. Journal of Guidance, Control, and Dynamics, 24(4):739–745, July 2001.

[15] the Kaguya project team, Manabu Kato, Susumu Sasaki, and Yoshisada Takizawa. The Kaguya Mission Overview. Space Science Reviews, 154(1-4):3–19, July 2010.

[16] D. A. Vallado. Fundamentals of Astrodynamics and Applications. Springer, May 2007.

[17] B. F. Villac and D. J. Scheeres. New class of optimal plane change maneuvers. Journal of guidance, control, and dynamics, 26(5):750–757, 2003.

[18] Matthew Paul Wilkins, Christian Bruccoleri, and Daniele Mortari. Constellation Design Using Flower Constellations. Paper AAS, pages 04–208, 2004.

[19] Maria T. Zuber, David E. Smith, Michael M. Watkins, Sami W. Asmar, Alexander S. Konopliv, Frank G. Lemoine, H. Jay Melosh, Gregory A. Neumann, Roger J. Phillips, Sean C. Solomon, and others. Gravity field of the Moon from the Gravity Recovery and Interior Laboratory (GRAIL) mission. Science, 339(6120):668–671, 2013.